



National Library  
of Canada

Bibliothèque nationale  
du Canada

Canadian Theses Service

Service des thèses canadiennes

Ottawa, Canada  
K1A 0N4

## NOTICE

The quality of this microform is heavily dependent upon the quality of the original thesis submitted for microfilming. Every effort has been made to ensure the highest quality of reproduction possible.

If pages are missing, contact the university which granted the degree.

Some pages may have indistinct print especially if the original pages were typed with a poor typewriter ribbon or if the university sent us an inferior photocopy.

Previously copyrighted materials (journal articles, published tests, etc.) are not filmed.

Reproduction in full or in part of this microform is governed by the Canadian Copyright Act, R.S.C. 1970, c. C-30.

## AVIS

La qualité de cette microforme dépend grandement de la qualité de la thèse soumise au microfilmage. Nous avons tout fait pour assurer une qualité supérieure de reproduction.

S'il manque des pages, veuillez communiquer avec l'université qui a conféré le grade.

La qualité d'impression de certaines pages peut laisser à désirer, surtout si les pages originales ont été dactylographiées à l'aide d'un ruban usé ou si l'université nous a fait parvenir une photocopie de qualité inférieure.

Les documents qui font déjà l'objet d'un droit d'auteur (articles de revue, tests publiés, etc.) ne sont pas microfilmés.

La reproduction, même partielle, de cette microforme est soumise à la Loi canadienne sur le droit d'auteur, SRC 1970, c. C-30.

Reactions in the  $MCl/SnF_2$  Systems ( $M=Na, K$  and  $NH_4$ ):  
Characterization of the Products  
and Crystal Structure of  
 $(NH_4)_3Sn_5F_{10}Cl_3$

Korzior Kwok Sik Tam

A Thesis

in

The Department

of

~~Chemistry~~ Chemistry

Presented in Partial Fulfillment of the Requirements  
for the Degree of Master of Science at  
Concordia University  
Montréal, Québec, Canada

March 1988

© Korzior Kwok Sik Tam, 1988

Permission has been granted to the National Library of Canada to microfilm this thesis and to lend or sell copies of the film.

The author (copyright owner) has reserved other publication rights, and neither the thesis nor extensive extracts from it may be printed or otherwise reproduced without his/her written permission.

L'autorisation a été accordée à la Bibliothèque nationale du Canada de microfilmer cette thèse et de prêter ou de vendre des exemplaires du film.

L'auteur (titulaire du droit d'auteur) se réserve les autres droits de publication; ni la thèse ni de longs extraits de celle-ci ne doivent être imprimés ou autrement reproduits sans son autorisation écrite.

ISBN 0-315-44239-5

## ABSTRACT

Reactions in the  $MCl/SnF_2$  Systems ( $M = Na, K, \text{ and } NH_4$ ):  
Characterization of the Products and Crystal Structure of  
 $(NH_4)_3Sn_5F_{10}Cl_3$

Korzior Kwok Sik Tam

The reactions between  $SnF_2$  and  $MCl$  ( $M = Na, K, \text{ and } NH_4$ ) in aqueous solution have been investigated. The three systems, with substitution of different alkali metals (or  $NH_4$ ) in the alkali metal chloride as listed, are extensions for previous publications by earlier workers in research areas related to divalent tin halides and their chemistry. The study was undertaken as an attempt to rationalize the difference in physical properties and crystal structures, as observed when  $MF$ ,  $MBr$ , and  $MI$  are replaced by  $MCl$ . ( $SnF_2$  with  $MF$ ,  $MBr$ , and  $MI$  were the original works by earlier researchers.)

New compounds have been obtained and identified. Two of them have been determined in terms of stoichiometry. They are  $(NH_4)_3Sn_5F_{10}Cl_3$  and  $K_3Sn_5F_{10}Cl_3$ , respectively. The crystal structure of the former compound has been determined. This compound crystallizes in the space group  $Bmmb$ , with unit-cell dimensions of  $a = 4.401 \text{ \AA}$ ,  $b = 20.999 \text{ \AA}$ , and  $c = 19.794 \text{ \AA}$ . There are four repeating units per unit-cell and its calculated density is  $3.43 \text{ g.cm}^{-3}$ . Other physical parameters of these two new compounds are presented in this text.

$^{119}\text{Sn}$  Mössbauer spectroscopic results indicate that the two new species could be fluoride and/or chloride ion conductors, but they are highly unlikely to exhibit electronic type conduction. It has also been confirmed that, by  $^{119}\text{Sn}$  Mössbauer spectroscopy, the tin(II) lone pair of electrons in these new materials is stereoactive and has considerable  $p_z$  character.

It has also been demonstrated how  $^{119}\text{Sn}$  Mössbauer spectroscopy can be used to probe the electrical environment of tin, for a simple and unambiguous identification of the potential electrical properties of the materials. No direct measurement of the electric properties was carried out in this project.

## TABLE OF CONTENTS

	<u>Page</u>
ABSTRACT	iii
ACKNOWLEDGEMENTS	v
FIGURE CAPTIONS	vii
TABLE CAPTIONS	ix
1.0 GENERAL INTRODUCTION	1
1.1 The Chemistry of Tin	1
1.2 Stereochemistry of Divalent Tin	2
1.3 Published Reports on Stannous Fluoride with Different Halides of Alkali Metals	5
1.4 Description of This Research	8
2.0 EXPERIMENTAL PREPARATIONS	10
2.1 Reactions for Crystal Growth	10
2.2 Chemical Analyses	11
2.3 X-Ray Diffraction Studies	12
2.4 Structure Determination	12
2.5 Mössbauer Spectroscopic Experiments	13
2.6 Thermal Gravimetric Analyses	14
2.7 Other Physical Measurements	14
3.0 X-RAY CRYSTALLOGRAPHY	15
3.1 Basic Concepts	15
3.2 Crystals and Their Symmetry	19
3.3 The Reciprocal Lattice	21
3.4 Laue Symmetry	22
3.5 The Diffraction of X-ray by Crystals	24

3.6 The Principles of Crystal Structure Analysis	26
3.7 The Phase Problem	28
3.8 The Heavy Atom Method	32
3.9 The Direct Methods	34
3.10 Least Squares Refinement	36
4.0 $^{119}\text{Sn}$ TIN MÖSSBAUER SPECTROSCOPY AND ELECTRICAL	38
PROPERTIES OF STANNOUS HALIDES	
4.1 Resonant Absorption and Fluorescence	38
4.2 The Mössbauer Effect	39
4.3 Hyperfine Interactions	42
4.4 Electrical Properties of Divalent Tin Halides	45
5.0 EXPERIMENTAL RESULTS	51
5.1 Products Obtained from Reactions	51
5.2 Crystallographic Data for New Compounds from	53
$\text{NH}_4\text{Cl}/\text{SnF}_2$	
5.3 Crystallographic Data for New Compound from	55
$\text{KCl}/\text{SnF}_2$	
5.4 Chemical Analytical Results	56
5.5 Summary of Mössbauer Experiments	58
5.6 Thermal Gravimetric Analyses	58
5.7 Physical Constants of New Compounds	65
6.0 THE CRYSTAL STRUCTURE OF $(\text{NH}_4)_3\text{Sn}_5\text{F}_{10}\text{Cl}_3$	66
6.1 Method of Choice for Structure Determination	66
6.2 Coordination of the Atoms	71
6.3 Structural Arrangement of the Atoms	75
7.0 DISCUSSION	79
7.1 Results Interpretation	79

7.1.1 Crystallographic Study	79
7.1.2 Mössbauer Spectroscopic Analysis	81
7.2 Comparison between this Research and the Earlier Similar Systems	84
7.3 Effects of Different Halides on Physical Properties	85
7.4 Ionic Radii and Structural Analogies	86
7.5 Further Work	90
REFERENCES	94



### ACKNOWLEDGEMENTS

I would like to take this opportunity to thank the three members of my research committee, Dr. Dénès, Dr. Bird, and Dr. Colebrook, for their generous assistance given to me throughout this research.

I thank Dr. Dénès, who is my research director, for introducing me to interesting areas such as X-ray diffraction techniques, Mössbauer spectroscopy, and solid-state chemistry, to only mention a few. His guidance to me, from practical research disciplines to daily-life, throughout my graduate years of study, has been valuable.

It was Dr. Bird who gave me a complete course of X-ray crystallography and really stretched my knowledge in the field. There is no doubt about the fact that part of this research would have remained unsolved without his excellent knowhow in this area, which I truly admire.

I also thank Dr. Colebrook for giving me lectures on NMR spectroscopy. I strongly believe the knowledge I gained from his lectures would be an asset to my future career. His suggestions for this research have also been very helpful.

I am also grateful for the technical support from the Technical Staffs Unit of Concordia University.

Finally, the people I really have to thank most, are my parents. They patiently remind me my physical disability is not and should not be a barrier to any success. Of that I am truly convinced.

TO  
MY PARENTS  
AND  
THE DISABLED

## FIGURE CAPTIONS

FIGURE 1.1 The stereochemistry of: (a) a  $p^2$  hybrid, and of (b) an  $sp^2$  hybrid of tin(II)- orbitals.

FIGURE 1.2 Formation of adducts of molecular tin(II) compounds.

FIGURE 3.1 A space lattice.

FIGURE 3.2 A unit-cell.

FIGURE 3.3 Miller indices of: (a) (100), and (b) (222).

FIGURE 3.4 The relationship between a real and reciprocal two-dimensional lattice. (a) real lattice; (b) reciprocal lattice.

FIGURE 3.5 Diffraction by a set of planes (Bragg's Law).

FIGURE 4.1 Schematic diagram for a Mössbauer experimental set-up.

FIGURE 4.2 Mössbauer hyperfine interactions of: (a) electric monopole; (b) electric quadrupole.

FIGURE 4.3  $^{119}\text{Sn}$  Mössbauer spectra of tin(II) halide compounds, as a function of their electrical properties.

(a)  $\text{CaSnO}_3$  reference ( $\delta = 0$ ,  $\Delta = 0$ ); (b) ionic conductor or insulator fluorides ( $\delta \approx 3.5$ ,  $\Delta \approx 1.5$ ); (c) bromide or iodide semiconductor ( $\delta \approx 4.0$ ,  $\Delta \approx 0$ ); (d)  $\text{CsSnBr}_3$ ,  $T > 418 \text{ K}$ , metal-type conductor ( $\delta = 0$ ,  $\Delta \approx 0$ ).

FIGURE 5.1 The physical appearance of: (a)  $\text{NH}_4\text{Sn}_2\text{F}_4\text{Cl}$ / $(\text{NH}_4)_3\text{Sn}_5\text{F}_{10}\text{Cl}_3$ ; (b)  $\text{K}_3\text{Sn}_5\text{F}_{10}\text{Cl}_3$ .

FIGURE 5.2  $^{119}\text{Sn}$  Mössbauer spectra of the new products from  $\text{MCl/SnF}_2$  ( $\text{M} = \text{K}, \text{NH}_4$ ). The spectrum of  $\alpha\text{-SnF}_2$  is given for

comparison. (a)  $\alpha$ - $\text{SnF}_2$ ; (b)  $\text{K}_3\text{Sn}_5\text{F}_{10}\text{Cl}_3$  (crystal); (c)  $\text{K}_3\text{Sn}_5\text{F}_{10}\text{Cl}_3$  (powder, after grinding); (d)  $\text{NH}_4\text{Sn}_2\text{F}_4\text{Cl}/(\text{NH}_4)_3\text{Sn}_5\text{F}_{10}\text{Cl}_3$  (crystal); (e)  $\text{NH}_4\text{Sn}_2\text{F}_4\text{Cl}/(\text{NH}_4)_3\text{Sn}_5\text{F}_{10}\text{Cl}_3$  (powder, after grinding).

FIGURE 5.3 The thermogram of: (a)  $\text{K}_3\text{Sn}_5\text{F}_{10}\text{Cl}_3$ ; (b)  $\text{NH}_4\text{Sn}_2\text{F}_4\text{Cl}/(\text{NH}_4)_3\text{Sn}_5\text{F}_{10}\text{Cl}_3$ .

FIGURE 6.1 A unit-cell of  $(\text{NH}_4)_3\text{Sn}_5\text{F}_{10}\text{Cl}_3$ . (a)  $(\vec{b}, \vec{c})$  plane; (b)  $(\vec{a}, \vec{b})$  plane.

FIGURE 6.2 A stereoscopic pair of  $(\text{NH}_4)_3\text{Sn}_5\text{F}_{10}\text{Cl}_3$  unit-cells.

FIGURE 6.3 Coordination of: (a) Sn(1) ( $\text{sp}^3\text{d}$ ); (b) Sn(2) ( $\text{sp}^3\text{d}$ ); (c) Sn(3) ( $\text{sp}^3\text{d}^2$ ).

FIGURE 6.4 Schematic plot of a unit-cell of  $(\text{NH}_4)_3\text{Sn}_5\text{F}_{10}\text{Cl}_3$  on the  $(\vec{b}, \vec{c})$  plane.

FIGURE 7.1 Relationships between the cell of the trigonal  $\text{KSn}_2\text{F}_5$  and the orthorhombic cells of  $\text{M}_3\text{Sn}_5\text{F}_{10}\text{Cl}_3$  ( $\text{M} = \text{K}$  and  $\text{NH}_4$ ).

### TABLE CAPTIONS

TABLE 2.1 Parameters for the X-ray data collection of  $(\text{NH}_4)_3\text{Sn}_5\text{F}_{10}\text{Cl}_3$ .

TABLE 3.1 The seven crystal systems.

TABLE 3.2 Relations between lattice symbol and lattice points.

TABLE 3.3 Possible lattices that can be assigned to individual crystal system.

TABLE 3.4 The eleven Laue groups.

TABLE 5.1 Indexed X-ray powder pattern of  $\text{K}_3\text{Sn}_5\text{F}_{10}\text{Cl}_3$ .

TABLE 5.2 Mössbauer spectroscopic parameters for materials obtained from this research and other related compounds.

TABLE 5.3 Physical constants for the new materials.

TABLE 6.1 Final atomic coordinates and equivalent isotropic Debye-Waller factor for  $(\text{NH}_4)_3\text{Sn}_5\text{F}_{10}\text{Cl}_3$ .

TABLE 6.2 Anisotropic ellipsoids of thermal vibrations for  $(\text{NH}_4)_3\text{Sn}_5\text{F}_{10}\text{Cl}_3$ .

TABLE 6.3 Bond distances in  $(\text{NH}_4)_3\text{Sn}_5\text{F}_{10}\text{Cl}_3$ .

TABLE 6.4 Bond angles for  $(\text{NH}_4)_3\text{Sn}_5\text{F}_{10}\text{Cl}_3$ .

TABLE 7.1 Comparison of the unit-cells of  $\text{M}_3\text{Sn}_5\text{F}_{10}\text{Cl}_3$  and  $\text{KSn}_2\text{F}_5$  ( $\text{M} = \text{K}$  and  $\text{NH}_4$ ).

## 1.0 GENERAL INTRODUCTION

### 1.1 The Chemistry of Tin

Divalent tin-containing halides can exhibit peculiar physical properties (e.g. electrical) depending on the other cations present in the solid and the electronegativity of the halogen, which together, in turn, affect the electronic structure of the divalent tin. For divalent tin containing compounds, the electronic configuration of tin plays an important role in terms of the physical properties (1-7) and crystal structure of the compound.

Tin is an element that belongs to the group IV B of the periodic table. It has the outer electronic configuration  $5s^2 5p^2$ , or to be more precise, the complete configuration  $[\text{Kr}]4d^{10}5s^2 5p^2$ . Tin behaves somewhat like its congeners germanium and lead. It can form compounds either in the +2 or +4 oxidation states; however, its +2 oxidation state is more stable than that of  $\text{Ge}^{2+}$  and less than that of  $\text{Pb}^{2+}$ . This trend, known as "s and p subgroup trend", is due to the increasing electropositivity of the group IV element as one goes down the group. It results in a more metallic character of the elements, a higher degree of ionicity and a lower degree of stereoactivity of the lone pair of the group IV element in the +2 oxidation state.

The most obvious feature that can be used to compare the properties of the compounds of an element is the way its valence electrons are used in bonding. Since the properties and chemistry of many tetravalent tin compounds are well

known and have been well described elsewhere in literature (8-10), emphasis will be stressed on divalent tin compounds and their stereochemistry here. It is also due to the fact that the new compounds which have been identified throughout this research do not involve any tetravalent tin derivatives.

### 1.2 Stereochemistry of Divalent Tin

The general method of approach to discuss the chemistry of tin(II) compounds, is based essentially on the outer electronic configuration of the element in the +2 oxidation state (11). This method can also be used to relate the physical properties to many divalent tin compounds, and their crystal structures.

To study the bonding in tin(II) compounds, the use of only two of the valence shell electrons for bonding is considered. In other words, the outer electronic configuration of the element in its +2 oxidation state must contain a completely filled s orbital and empty p (as well as d) orbitals that can be used in compound formation.

On the basis of its outer electronic configuration, four possible ways for tin to form bonds in the +2 oxidation state are known and they are listed as below (11):

- (a) by loss of the two 5p electrons to form the stannous ion,  $\text{Sn}^{2+}$ ;
- (b) by the use of the two 5p electrons to form covalent bonds;

- (c) by complex formation, i.e. including the empty 5p and 5d orbitals in the hybridization as acceptor orbitals;
- (d) by overlap of a directed lone-pair orbital on the tin atom with an empty orbital on an acceptor species.

The following discussion only represents a general summary of the above four possible ways of divalent tin bond formation. It cannot serve as a standard text, and for this particular reason, readers are advised to consult original texts for a complete view.

As stated earlier, the ground state electronic configuration for tin is  $5s^2 5p^2$ , therefore, it can form covalent tin(II) compounds using its two unpaired p electrons. If the  $5s^2$  electrons do not participate in compound formation, then the bond angle in such a  $SnX_2$  molecule is expected to be  $90^\circ$ , as in FIGURE 1.1a.

However, the s electrons are usually incorporated into a  $sp^2$  hybridization, and as a direct consequence, the bond angle is about  $120^\circ$  (See FIGURE 1.1b). In fact, the bond angle is smaller than  $120^\circ$  because the lone pair-bonding pair repulsions are bigger than the bonding pair-bonding pair repulsions (VSEPR Rule Number 2).

Tin(II) chloride, for instance, in the gas phase has the structure shown in FIGURE 1.2a. The two  $sp^2$  orbitals in this case form covalent bonds to the chloride ions with one directional lone pair of electrons. In the case of tin(II) complex species, an extra empty p orbital which is of similar energy to those used in bonding, is involved in the



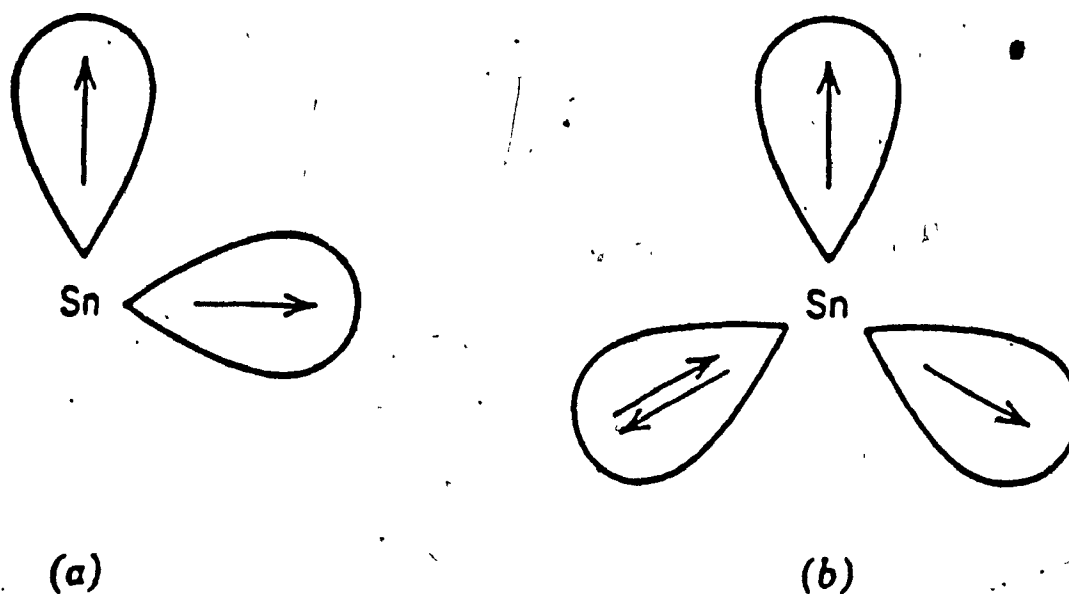


FIGURE 1.1 The stereochemistry of: a) a  $p^2$  hybrid and of b) an  $sp^2$  hybrid of tin(II) orbitals.

so-called complex compound formation. This extra empty p orbital is at right angle to the plane of the molecule (FIGURE 1.2b). Divalent tin compounds with considerable covalent bond character are expected to behave as a monofunctional acceptor toward suitable monodentate ligands, hence forming complexes of the type  $SnX_2 \cdot \text{ligand}$ . The stereochemistry of this type of divalent tin complex is based on the "overlapping" of the lone pair of electrons from the ligand with the empty p orbital of the tin. Molecules of this type are likely to be distorted in terms of molecular structure (FIGURE 1.2c).

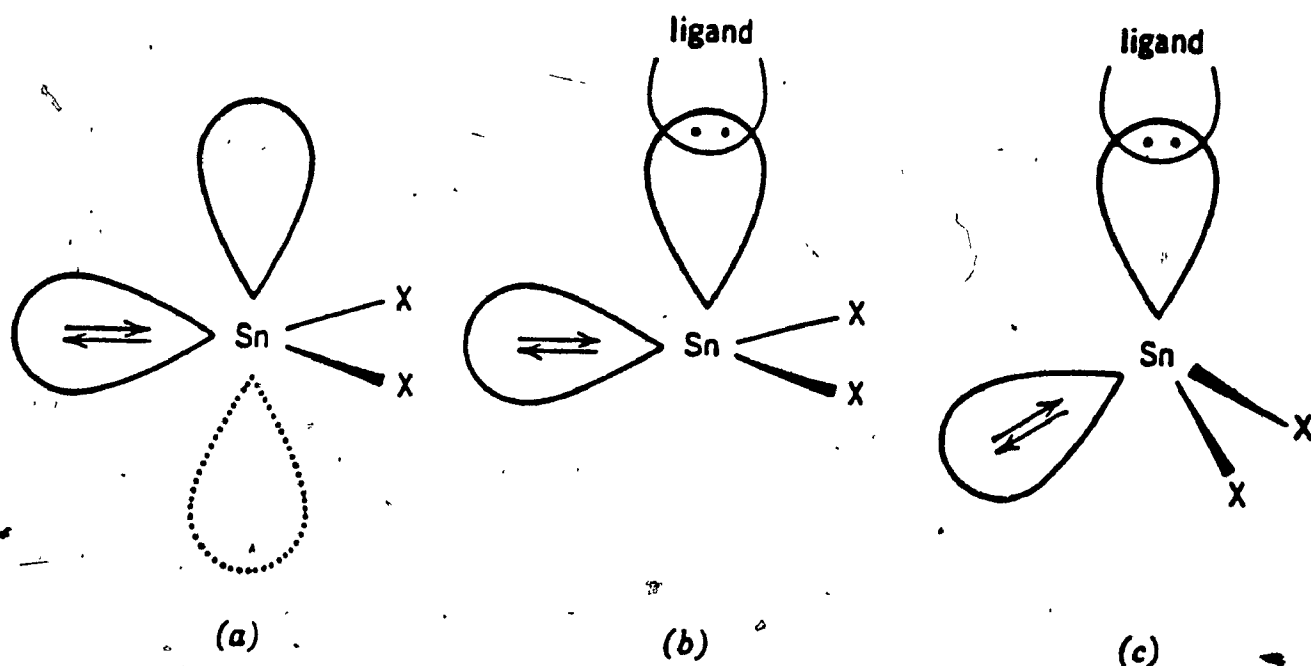


FIGURE 1.2 Formation of adducts of molecular tin(II) compounds.

The relative sizes of the divalent tin and fluoride (or oxide) ions should favour an octahedral coordination of tin. However, the presence of the hybridized non-bonding electron pair on tin (II) decreases the coordination number and strongly distorts the polyhedron of coordination of tin (12).

### 1.3 Published Reports on Stannous Fluoride with Different Halides of Alkali Metals

As stated at the beginning, divalent tin fluoride and its combinations with other halides of alkali metals give

rise to materials which can exhibit very diverse types of electrical properties. As a general rule, if the halide is fluoride, then the compounds obtained are fluoride ion conductors, while bromides and iodides give rise to semiconducting properties.

This section presents the previous studies and publications on stannous fluoride with other halides of alkali metals. It also presents materials involving band theories. Readers should refer to relevant texts where appropriate.

Divalent tin fluoride has been shown to increase the mobility of the fluoride ions in solids by several orders of magnitude (13),  $\text{PbSnF}_4$  and  $\text{BaSnF}_4$  being to date the best known fluoride ion conductors. In these compounds, a high energy gap prevents any significant long range electron mobility. On the other hand, for larger and less electronegative halogens, the energy gap between the valence and conduction bands is much lower, and hence giving rise to semiconducting properties, as in the cases of  $\text{CsSnCl}_3$  and  $\text{CsSnBr}_3$  (14), the latter of which even can exhibit metal-type conducting property at temperatures above 418 K (14).

Some of these properties have been observed in the compounds obtained by reaction of alkali metal halides  $\text{MX}$  with stannous fluoride  $\text{SnF}_2$ . Earlier studies of the reactions of the alkali metal fluorides  $\text{MF}$  with  $\text{SnF}_2$  in aqueous solutions were carried out by Kriegsmann and Kessler (15), Donaldson, and O'Donoghue (16), and Goost and Bergerhoff (17). More recent studies (18,19) have confirmed that

most of the compounds obtained belong to the  $\text{MSnF}_3$  or  $\text{MSn}_2\text{F}_5$  series and have provided some rationale of their crystallographic unit-cell. The crystal structure of only a few of these have been solved, viz.  $\text{NaSn}_2\text{F}_5$  (20),  $\text{KSn}_2\text{F}_5$  (21), and  $\text{NH}_4\text{SnF}_3$  (22-24). The crystal structure of two other compounds, with non-standard stoichiometry, viz.  $\text{KSnF}_3 \cdot 1/2\text{H}_2\text{O}$  (25) and  $\text{Na}_4\text{Sn}_3\text{F}_{10}$  (26), have also been reported. However, these were obtained on a unique crystal and there is no evidence that a batch of such stoichiometry was ever isolated. Electrical conductivity and  $^{19}\text{F}$  nuclear relaxation measurements have shown the high mobility of fluoride ions in the  $\text{MSn}_2\text{F}_5$  compounds for  $\text{M} = \text{K}, \text{Tl}, \text{NH}_4$ ; and  $\text{Rb}$  (21, 27-30).

There are fewer studies on the  $\text{SnF}_2/\text{MX}$  ( $\text{X} = \text{Br}$  and  $\text{I}$ ) systems. In the system  $\text{CsSnF}_3\text{-CsSnX}_3$  ( $\text{X} = \text{Br}$  and  $\text{I}$ ), distinct phases of  $\text{CsSnF}_2\text{X}$  have been reported as well as a continuous range of coloured solid solutions  $\text{CsSnF}_{3-n}\text{X}_n$  ( $n > 1.5$ ) with cubic ( $\text{X} = \text{Br}$ ) and orthorhombic ( $\text{X} = \text{I}$ ) unit-cells (31). Finally, a study on the phases obtained in the  $\text{SnF}_2/\text{MI}$  systems ( $\text{M} = \text{Na}, \text{K}, \text{Rb}$ , and  $\text{NH}_4$ ) shows the existence of three distinct stoichiometries, namely  $\text{MSnF}_2\text{I}$ ,  $\text{MSn}_2\text{F}_4\text{I}$ , and  $\text{MSn}_3\text{F}_6\text{I}$  (32). For reactions between  $\text{SnF}_2$  and alkali metal chlorides, only a study with  $\text{CsCl}$  has been reported (31) and the following species have been isolated:  $\text{CsSnF}_2\text{Cl}$ ,  $\text{Cs}_2\text{Sn}_2\text{F}_3\text{Cl}_3$ , and  $\text{CsSnFCl}_2$ . All of the above compounds containing both fluorine and another halogen, are strongly colored. This has been attributed mostly to low

energy conduction bands giving rise to strong optical absorption and electronic conductivity (semiconducting type).

#### 1.4 Description of this Research

There is no report in the literature on the study of  $\text{SnF}_2/\text{MCl}$  systems, except for  $\text{M} = \text{Cs}$  (31). The results obtained throughout this research, upon reactions between  $\text{SnF}_2$  and  $\text{MCl}$  ( $\text{M} = \text{Na}$ ,  $\text{K}$ , and  $\text{NH}_4$ ), are presented here. This study was undertaken in order to try to isolate new compounds in these systems, and to study the influence of the chloride ion on the structural and electrical properties. This appears to be interesting as the more electronegative fluorine gives rise to white ionic conducting materials and the less electronegative bromine and iodine result in semiconducting and strongly coloured compounds.

The new compounds obtained from the present study have been confirmed as possible ionic conductor either of fluoride-type nature or mixed-halide type. Such identification can be achieved unambiguously using  $^{119}\text{Sn}$  Mössbauer spectroscopy as an analytical tool, the technique of which will be focused on in detail later in the text. However, no direct measurement of the electric properties of our materials was undertaken in this project.

The crystal structure of one of the new species has been determined. This structure will be presented, along with its physical parameters. Also, physical constants of

other new materials resulted from this research are also  
underlined.

## 2.0 EXPERIMENTAL PREPARATION

### 2.1 Reactions for Crystal Growth

Stannous fluoride  $\text{SnF}_2$  was supplied by Ozark-Mahoning. Sodium chloride ( $\text{NaCl}$ ), potassium chloride ( $\text{KCl}$ ), and ammonium chloride ( $\text{NH}_4\text{Cl}$ ) were obtained from Anachemia.

The chemicals were used without further purification. In the case of aqueous state reactions, they were performed with doubly deionized water contained in teflon or pyrex beakers. When pyrex beakers were used, the inside of the beaker was covered with a polyethylene film (of the type used for wrapping food) to avoid etching of the glass by fluoride ions. This has also the big advantage, over teflon beakers, which do not need this protection, to make much easier the collection of crystals, which are otherwise often stuck to the bottom of the beaker and are hard to remove without damaging them. After dissolving  $\text{SnF}_2$  and the chloride in warm water, the solutions were allowed to cool to room temperature. After cooling, a few drops of 48 % aqueous  $\text{HF}$  were added to prevent hydrolysis of tin(II) and a piece of tin metal was immersed in the solution to slow down oxidation to tin(IV) (33,34). Then the solutions were allowed to evaporate at room temperature. After a few days, long crystals of needle-shape were formed, together with crystals of excess starting materials and/or byproducts, and a white powder, which was usually a complex mixture.

The crystals were removed from the solution allowed to dry in air at room temperature, and stored in a polyethylene

container. The remaining solutions were allowed to evaporate further and often yielded a second crop of crystals.

Seven reactions with different stoichiometries were carried out as follows:

- (a)  $\text{SnF}_2 + \text{MCl}$
- (b)  $\text{SnF}_2 + 2\text{MCl}$
- (c)  $\text{SnF}_2 + 5\text{MCl}$
- (d)  $\text{SnF}_2 + 10\text{MCl}$
- (e)  $2\text{SnF}_2 + \text{MCl}$
- (f)  $5\text{SnF}_2 + \text{MCl}$
- (g)  $10\text{SnF}_2 + \text{MCl}$

where M = Na, K, and  $\text{NH}_4$ .

## 2.2 Chemical Analyses

Metal analysis was performed on a Perkin-Elmer 503 atomic absorption spectrometer. The samples were dissolved in 20 % HCl (v/v) as to avoid any tin loss (35), and they were measured while they were still fresh.

The amount of ammonium was determined by decomposing the sample in boiling aqueous solution upon the addition of a strong base in excess (NaOH). The ammonia evolved was neutralized in an excess acidic solution and the excess acid was back-titrated with a standard base (36).

The quantitative analyses for the halides were tested by two techniques, the potentiometric method (i.e. selective ionic electrodes of fluoride and chloride type) and the



pyrohydrolytic method of determination of halides (37), respectively.

### 2.3 X-ray Diffraction Studies

Single crystals were selected and mounted on a goniometer head. The unit-cell constants and symmetry elements were obtained by taking oscillation, Weissenberg, precession, and Laue photographs, using the  $K\alpha$  radiation of molybdenum ( $\lambda = 0.7107 \text{ \AA}$ ). Ground single crystals and powders were identified by X-ray powder diffraction technique, performed on a Picker diffractometer, using Ni-filtered  $K\alpha$  radiation of copper ( $\lambda = 1.5418 \text{ \AA}$ ).

### 2.4 Structure Determination

Single crystal intensity data were collected using a Picker Nuclear Facs-1 four circle diffractometer, coupled with a Picker Nuclear 2861 radiation analyzer. The X-ray source was produced by a Mo X-ray tube powered by a Picker Nuclear model 6238E X-ray generator. Data intensities were detected using a (Tl)NaI scintillation counter and were saved on a DP 8a Digital Equipment computer. The details of the data collection are given in TABLE 2.1.

Programs concerning data collection were from the NRC of Canada Single Crystal Data Collection Package.

Structure factor calculations and least squares refinements were accomplished by using the program LSTSQ (38) and all Fourier syntheses were done by the program FOURR (39).

TABLE 2.1

Parameters for the X-ray data collection of  $(\text{NH}_4)_3\text{Sn}_5\text{F}_{10}\text{Cl}_3$ 

Wavelength $\text{MoK}_\alpha$ :	0.71063 Å
$\theta$ range:	3.50° - 55.00°
h:	0 - 5
k:	0 - 23
l:	0 - 22
Standard reflections:	12 0 0, 0 6 0, 0 0 8
Total number of reflections collected:	1426
Number of reflections within $3\sigma$ :	660
Final R:	0.0982
Final $R_w$ :	0.1894

The program DISPOW (40) was used to compute the various interatomic distances and to calculate bond angles between atoms.

Graphics of crystal structure were produced by using the program ORTEP (41) coupled to a X-Y coordinate plotter.

## 2.5 Mössbauer Spectroscopic Experiments

For  $^{119}\text{Sn}$  Mössbauer spectroscopy, the Doppler velocity required was achieved by using an Elscint driving system working in the constant acceleration mode. The radiation source was a  $\text{Ca}^{119\text{m}}\text{SnO}_3$  15 mCi gamma-ray source supplied by Amersham. The gamma-ray beam transmitted by the thin absorber sample was measured by a (Tl)NaI scintillation counter, obtained from Harshaw. The spectra, recorded for

powdered and single crystal samples, were accumulated in a 2 K Tracor Northern 7200 multichannel analyzer operating in the multiscaling mode. The spectra were transferred to an IBM Compatible Personal Computer and saved on diskette. Computer fitting was performed on a Cyber 835 main-frame computer using the GMFP5 software of Ruebenbauer and Birchall (42), as modified by Dénès (43). The samples were about 400 mg of crystals or finely ground powder pressed in a teflon holder.

#### 2.6 Thermal Gravimetric Analyses

TGA experiments were carried out on a Perkin-Elmer TGS-2 thermobalance under a continuous flow of nitrogen. Seven milligrams of sample were heated in a platinum crucible at a linear rate of 10 °C rise per minute, and the weight of the sample was recorded versus its temperature.

#### 2.7 Other Physical Measurements

Melting points were determined on a standard Gallenkamp melting point apparatus. Pictures of the crystals were taken on an optical microscope, Carl Unïversal R. microscope from Zeiss, equipped with a Polaroid camera. Bulk density measurements were carried out on a collection of single crystals, about 200 mg, by the Archimedeian method, in carbon tetrachloride.

### 3.0 X-RAY CRYSTALLOGRAPHY

The purpose of this chapter is to present some fundamentals of X-ray crystallography. Further details can be found in numerous crystallography textbooks (44,45,46).

#### 3.1 Basic Concepts

A crystal contains atoms arranged in a repetitive three-dimensional pattern. If each repeat unit of this pattern, which may be an atom or a group of atoms, is taken as a point then a three-dimensional point lattice is created. A space lattice such as that shown in FIGURE 3.1 is obtained when lines are drawn connecting the points of the point lattice.

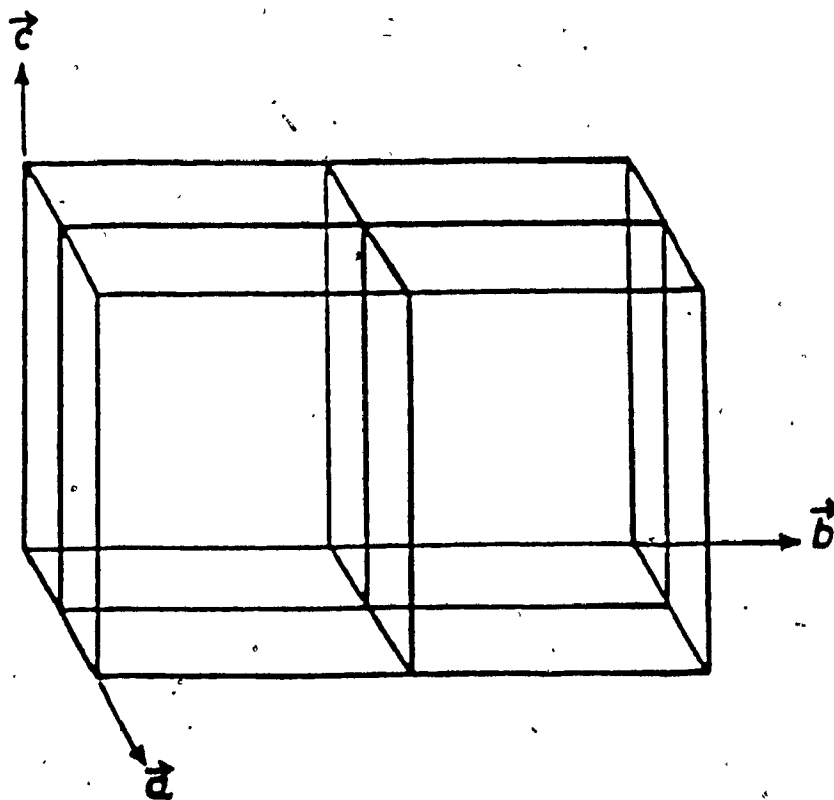


FIGURE 3.1 A space lattice.

It can be seen that the space lattice is composed of box-like units, the dimensions of which are fixed by the length of the space lattice between the points in the three non-coplanar directions  $\vec{a}$ ,  $\vec{b}$ , and  $\vec{c}$ . These small boxes are known as unit-cells and the crystal structure has a periodicity (based on the contents of these cells) represented by the translation of the original unit of pattern along the three directions  $\vec{a}$ ,  $\vec{b}$ , and  $\vec{c}$ .

The unit lengths along these three directions, together with the three angles, subtended by every two of them, are referred to as unit-cell parameters (See FIGURE 3.2).

The way to describe a plane or any plane in a unit-cell is by Miller indices. If a plane makes intercepts  $h$ ,  $k$ , and  $l$  (where  $h$ ,  $k$ , and  $l$ , are whole numbers or zero), at three crystal axes,  $\vec{a}$ ,  $\vec{b}$ , and  $\vec{c}$ , respectively, then the fractional length in each case are  $a/h$ ,  $b/k$ , and  $c/l$ , as in the written

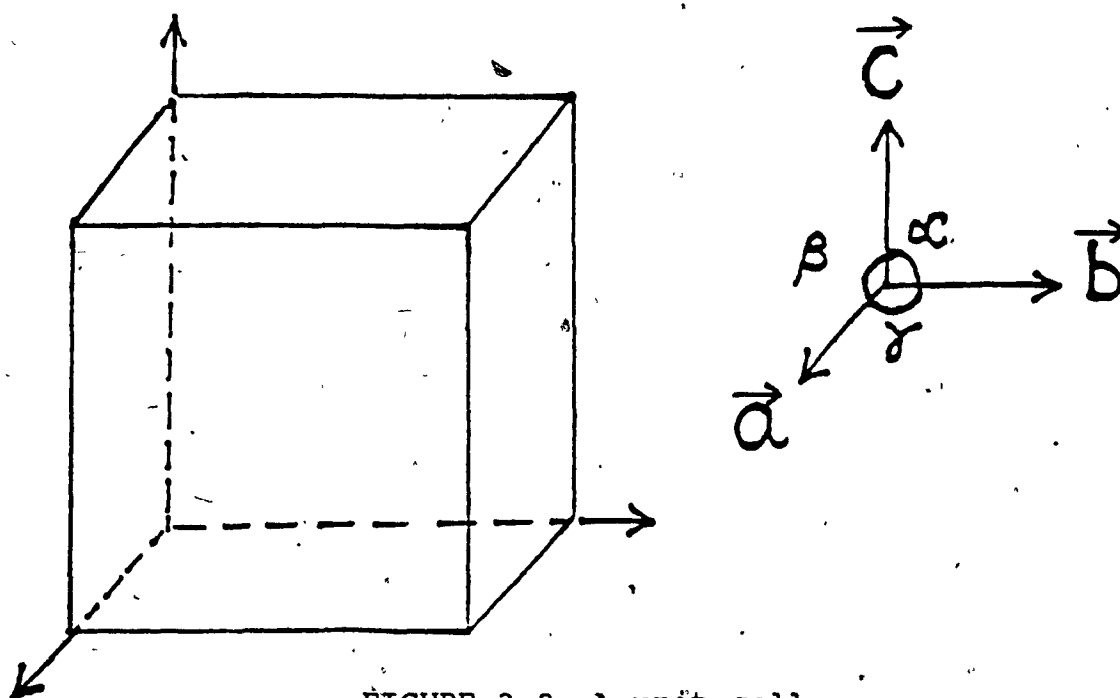


FIGURE 3.2 A unit-cell.

order. To define such a plane, these three fractional lengths are expressed in their reciprocal form. For example, a plane which makes intercepts at half  $a$ , half  $b$ , and half  $c$ , has Miller indices  $(222)$ ; similarly, when a plane cuts  $a$  at a third,  $b$  at a quarter, and  $c$  at a half, its Miller indices are  $(342)$ . Miller indices of the types  $(h00)$ ,  $(0k0)$ , and  $(00l)$ ;  $(hko)$ ,  $(hol)$ , and  $(okl)$ , are also valid. They represent planes which lie perpendicular to a particular crystal axis and planes which make only two intercepts respectively (See FIGURE 3.3).

Crystals are differentiated into seven systems and the relationships of the axes and angles in each case are listed in TABLE 3.1.

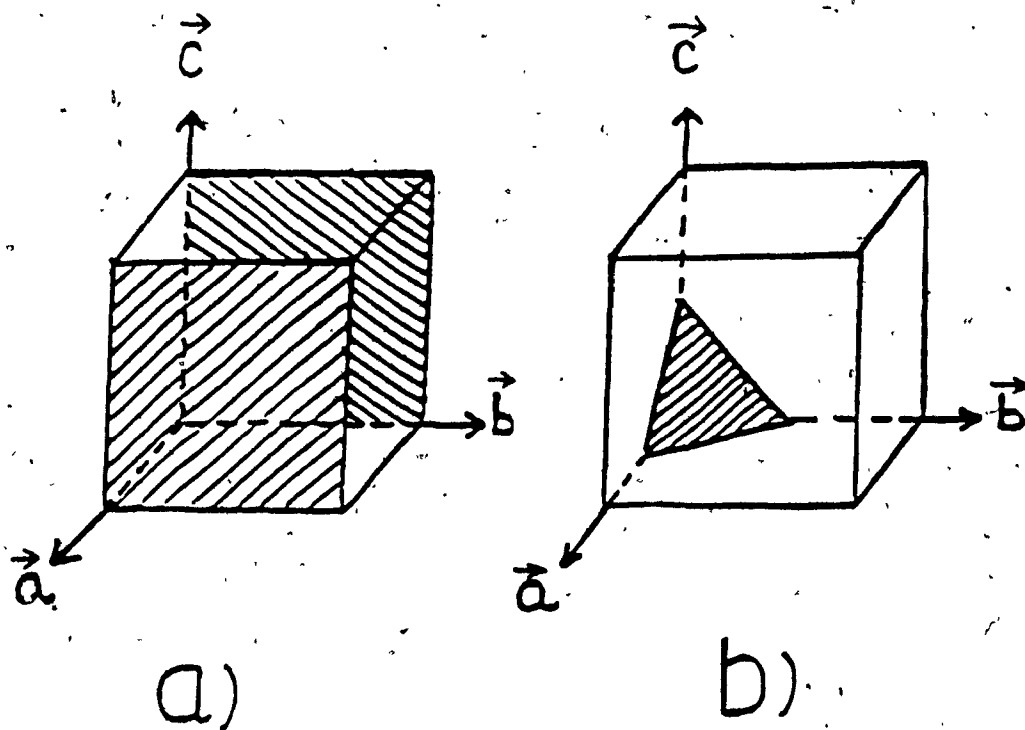


FIGURE 3.3. Miller indices of: a)  $(100)$  and b)  $(222)$ .

In the discussion so far, only primitive unit-cells have been considered, that is the lattice points are at the corners of the unit-cell. The monoclinic, orthorhombic, tetragonal, and cubic, systems can also have lattices, where lattice points exist at the center of faces, or in the

TABLE 3.1  
The seven crystal systems

<u>System</u>	<u>Axial Relations</u>	<u>Angular Relations</u>
Triclinic	$a \neq b \neq c$	$\alpha \neq \beta \neq \gamma \neq 90^\circ$
Monoclinic	$a \neq b \neq c$	$\alpha = \gamma = 90^\circ \neq \beta$
Orthorhombic	$a \neq b \neq c$	$\alpha = \beta = \gamma = 90^\circ$
Tetragonal	$a = b \neq c$	$\alpha = \beta = \gamma = 90^\circ$
Hexagonal	$a = b \neq c$	$\alpha = \beta = 90^\circ; \gamma = 120^\circ$
Cubic	$a = b = c$	$\alpha = \beta = \gamma = 90^\circ$
Trigonal (Rhombohedral)	$a = b = c$	$\alpha = \beta = \gamma \neq 90^\circ$

middle of the body diagonal, as well as at the corners of the unit-cell. These are known as centered lattices, of which there are seven, and together with the seven primitive lattices, they constitute the fourteen Bravais lattices. Each lattice type is represented by a lattice symbol and is summarized in TABLE 3.2. TABLE 3.3 shows the distribution of the lattice types among the crystal systems.

### 3.2 Crystals and their Symmetry

The ability of crystals to diffract X-rays was first observed by Von Laue in 1912, and hence marked the offset in the development of crystallography. His observation led to the fact that crystals must have a regular three-dimensional structural array, or in simpler words, atoms are arranged in a repetitive and regular fashion in a crystal.

TABLE 3.2  
Relations between lattice symbol and lattice points

<u>Lattice Symbol</u>	<u>Lattice Points</u>
P (primitive)	All corners
I (inner = body centered)	All corners and center of cell
A (centered on two faces)	All corners and A face-centered
B (centered on two faces)	All corners and B face-centered
C (centered on two faces)	All corners and C face-centered
F (centered on all faces)	All corners and all face-centered
R (rhombohedral)	All corners

A dictionary definition of symmetry is "a disposition (i.e. arrangement) of parts". In the case of crystals, it is possible to describe both their internal and external symmetry, in terms of a limited number of symmetry elements. The possession of symmetry by an object is usually recognized when the performance of some geometrical operation



TABLE 3.3  
Possible lattices that can be assigned to  
individual crystal system

<u>Crystal System</u>	<u>Possible Lattices</u>
Triclinic	P
Monoclinic	P, C
Orthorhombic	P, C, F, I
Tetragonal	P, I
Hexagonal	P
Cubic	P, F, I
Trigonal	R

leads to self-coincidence of the object. The operation may be reflection across a plane or rotation about an n-fold axis, where  $2\pi/n$  is the angle of rotation leading to self-coincidence.

In brief, there are two kinds of symmetry elements in crystallography. One of them has translational operation involved, while the other does not.

Symmetry elements without translation are represented by the following:

- (a) center of symmetry:  $\bar{1}(x,y,z \rightarrow \bar{x},\bar{y},\bar{z})$
- (b) mirror planes:  $m$
- (c) rotation axes: 1, 2, 3, 4, and 6
- (d) inversion axes:  $\bar{1}, \bar{2}, \bar{3}, \bar{4}, \text{ and } \bar{6}$  (rotation and center of symmetry)

There are a total of thirty-two possible groupings of the above symmetry elements, giving rise to the so-called "thirty-two point groups" in crystallography.

There are only two types of symmetry elements with translational operation, represented by screw axes and glide planes, respectively. A screw axis combines rotation about a 2-, 3-, 4-, or 6-fold axis, with translation in the direction of the axis. The translation distance is a multiple of  $1/2$ ,  $1/3$ ,  $1/4$ , or  $1/6$ , of the line-lattice translation. Therefore, a two-fold screw axis is symbolized as  $2_1$  and would result in rotation about a two-fold axis and translation by  $1/2$  the repeat distance of the axis. The operation of a glide plane combines reflection across a plane with translation parallel to the plane. The distance of translation is equal to a certain fraction of the translation that produces the line lattice.

Screw axes and glide planes, when taken in conjunction with the point group symmetry operations, result in 230 possible space groups to describe the symmetry of crystal lattices.

### 3.3 The Reciprocal Lattice

So far, only the space lattice of a crystal in real space has been considered, i.e. the real lattice. It is possible for every real lattice to construct a reciprocal lattice. (The concept of the reciprocal lattice was used by P.P. Ewald and extended by M. Von Laue (1913) to describe

the relationship between crystal structure and diffraction pattern.) To construct a reciprocal lattice, any point of the real lattice is taken as an origin, from which lines are drawn perpendicular to all sets of real lattice planes. Reciprocal lattice points arise on these lines at distances inversely proportional to the spacings of the real planes, and also fall on sets of parallel planes. The indices of a reciprocal lattice point,  $(hkl)$ , are the same as the indices of the planes in the real lattice that the point represents. It should be noted that the interplanar spacing in the real lattice, and not the distance between lattice points, is the parameter which gives the distance between lattice points in reciprocal space. FIGURE 3.4 shows the relationship between a real two-dimensional lattice and its corresponding reciprocal lattice. A three-dimensional lattice simply consists of layers of two-dimensional lattices one above the other, the actual relationship between these layers being dependent on the crystal system.

Conventionally, the axes and angles of a unit-cell in a real lattice are labelled  $\vec{a}$ ,  $\vec{b}$ ,  $\vec{c}$ , and  $\alpha$ ,  $\beta$ ,  $\gamma$ , respectively. In a reciprocal lattice, they are labelled  $\vec{a}^*$ ,  $\vec{b}^*$ ,  $\vec{c}^*$ , and  $\alpha^*$ ,  $\beta^*$ ,  $\gamma^*$ , respectively.

### 3.4 Laue Symmetry.

The symmetry of diffraction effect from a crystal at first glance may be thought to reflect the point group symmetry of the crystal under study. However, the

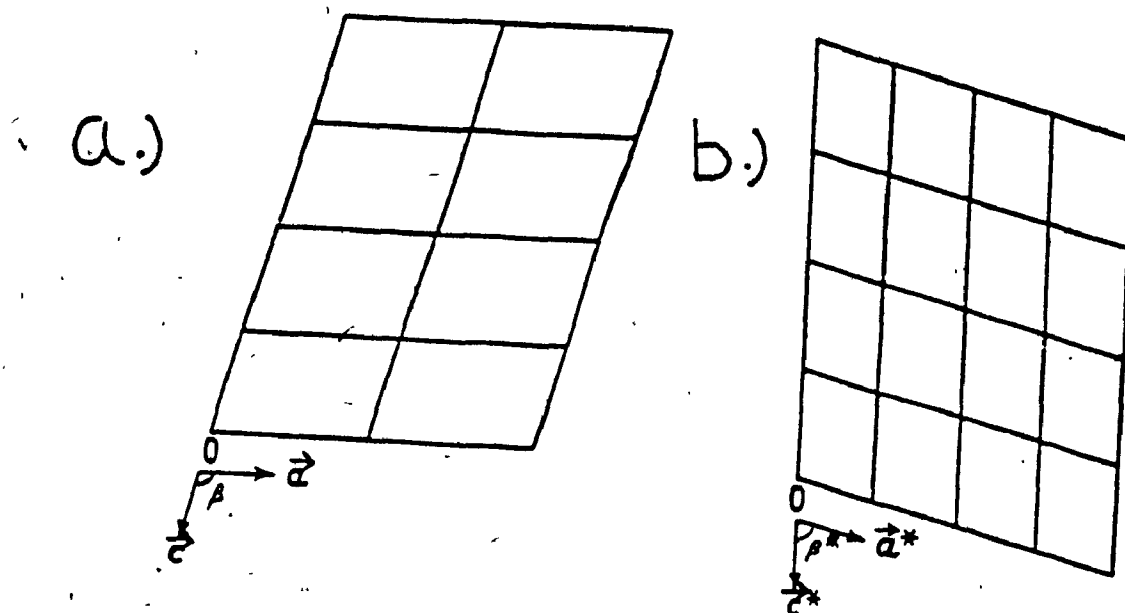


FIGURE 3.4 The relationships between a real and reciprocal two-dimensional lattice: a) real lattice; b) reciprocal lattice.

diffraction pattern differs from the point group symmetry in one important respect; it always has a center of symmetry even when one is not present in the crystal, since reflection  $hkl$  and  $\overline{hkl}$  are identical (Friedel's Law).

The diffraction pattern symmetry is therefore that of the crystal point group, together with a center of symmetry. In this way, the 32 point groups, when applied to diffraction patterns, reduce to 11 centrosymmetric point groups or Laue groups, as summarized in TABLE 3.4.

TABLE 3.4  
The eleven Laue groups

<u>Crystal System</u>	<u>Laue Symmetry</u>
Triclinic	$\bar{1}$
Monoclinic	$2/m$
Orthorhombic	$mmm$
Tetragonal	$4/m; 4/mmm$
Trigonal	$\bar{3}; \bar{3}m$
Hexagonal	$6/m; 6/mmm$
Cubic	$m\bar{3}; m\bar{3}m$

The significance of this can be seen by considering the monoclinic system. In this system, there are three possible point groups ( $2$ ,  $m$ , and  $2/m$ , respectively). The symmetry of the X-ray diffraction pattern produced by each of their point groups would be  $2/m$ ; the three groups could not be distinguished from one another by their diffraction pattern.

### 3.5 The Diffraction of X-ray by Crystals.

As mentioned previously, X-rays are diffracted by crystals, the next step is to describe how one may deduce from the diffraction pattern of a crystal, not only the dimensions and symmetry of the unit-cell, but also the relative positions of the atoms in the crystal.

Wave motion may produce diffraction effects when it interacts with any objects, which have a regular and repetitive structural configuration, if the wavelength

associated with the wave function is in the same order of the repeat distance, the periodicity of the object.

In FIGURE 3.5, a two-dimensional lattice is shown in order to demonstrate how a crystal diffracts an incident beam of X-rays (Bragg's Law).

For reinforcement to occur when the X-ray beam is reflected by the crystal, there must be a whole number of wavelength differences in the path lengths of the rays scattered by successive planes and the incident angle  $\theta_i$  must be equal to the diffracted angle  $\theta_d$ . As illustrated in the diagram, this means that  $ABC$  must be a whole number of wavelengths.

$$\text{Now } AB = AC = d \sin \theta; AB + AC = 2d \sin \theta.$$

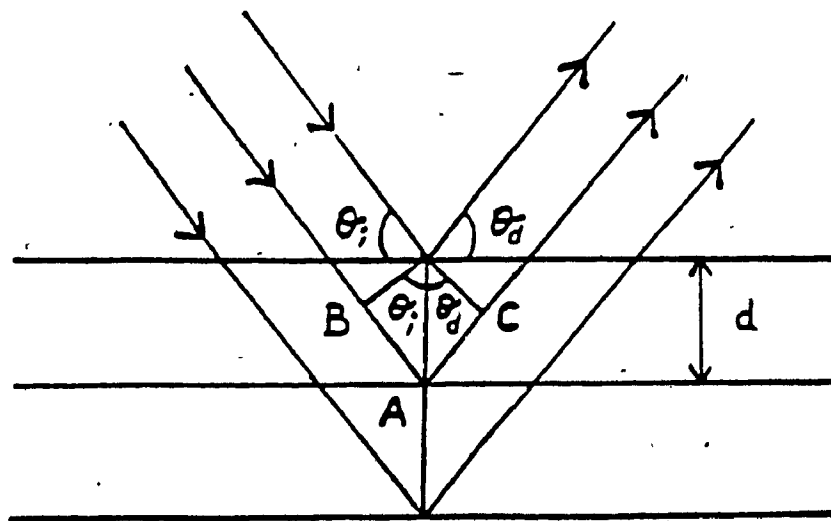


FIGURE 3.5 Diffraction by a set of planes (Bragg's Law).

with  $\theta = \theta_i = \theta_d$  is the Bragg angle and  $d$  is called the interplanar spacing.

For reinforcement,  $n\lambda = 2d\sin\theta$ , where  $n$  is a whole number. This is Bragg's Law, and every time a reflection occurs, this equation has been satisfied by the geometry of the crystal and the incident X-ray beam.

### 3.6 The Principles of Crystal-Structure Analysis

The first step for crystal-structure analysis is to measure the relative intensities of a large number of reflections and the reason for this is easy to understand. As indicated by Bragg's Law, the  $\theta$  value depends only on  $d(hkl)$ , the perpendicular spacing of each plane. As a result, the positions of the spots on an X-ray picture allow the determination of the unit-cell parameters. X-rays are scattered by electrons, so the intensity of a particular  $(hkl)$  reflection will depend upon how closely the electrons are concentrated on the planes of that particular set. Therefore, by comparing the relative intensities of a large number of reflections, it may be possible to have an idea on the positions of the electron density blobs, which constitute the atoms in a crystal.

The quantity carrying the intensity information is the structure factor, expressed as  $F(hkl)$ . The structure factor has both a magnitude (amplitude) and a phase (relative to the origin or the unit-cell). The magnitude of the structure factor,  $|F(hkl)|$ , is the ratio of the amplitude of the

radiation scattered in a particular direction by the contents of one unit-cell to that scattered by an electron at the origin of the unit-cell under the same conditions.

The structure factor depends on the following:

- (a) the nature of the scattering material;
- (b) the arrangement of the scattering material (including thermal motion);
- (c) the direction of scattering.

The experimentally measured (observed) structure factor amplitudes are denoted by  $|F_o(hkl)|$ ; those calculated for a model of the structure are designated as  $|F_c(hkl)|$ . The structure factor is the Fourier transform of the unit-cell contents sampled at reciprocal lattice points,  $h$ ,  $k$ , and  $l$ .

If the structure of a crystal is known, it is always possible to calculate the structure factor,  $F_c(hkl)$ , by the following expression:

$$F_c(hkl) = \sum_j f_j \phi(x_j, y_j, z_j, P_j, \dots) \quad (3.1)$$

In the above expression,  $x_j$ ,  $y_j$ , and  $z_j$ , are the fractional coordinates of each  $j$ th atom, and  $P_j$  represents the parameter(s) responsible for its vibrational motions. The summation is to be taken over all the atoms in a unit-cell, and  $\phi$  means "a function of". And since X-rays are scattered by electrons, therefore the term  $f_j$ , the atomic scattering function for the  $j$ th atom, has to be introduced in the expression.



The numerical values obtained from the expression have signs associated with them; however, the experimental measured structure factors do not have such signs. The ultimate evidence of the validity of a crystal-structure analysis is a good agreement between the  $|F_O(hkl)|$  and the  $|F_C(hkl)|$ .

### 3.7 The Phase Problem

In order to obtain an image of the scattering matter (the crystal) in three dimensions (the electron distribution), it is necessary to perform a three-dimensional Fourier synthesis. Fourier series are used because they can be applied to a description of regularly periodic functions, and crystals contain periodic distributions of scattering matter. The number of electrons per unit volume or electron density at any point  $x, y, z$ , represented by  $\rho(xyz)$ , is given as follows:

$$\rho(xyz) = (1/V_C) \sum_{\text{all } h, k, l} F(hkl) \exp[-2\pi i(hx + ky + lz)] \quad (3.2)$$

where  $V_C$  is the volume of the unit-cell and  $F(hkl)$  is the structure factor for the particular set of indices  $h, k$ , and  $l$ . The triple summation is over all values of the indices  $h, k$ , and  $l$ . The amplitude of the structure factor is easily derived from the intensity of the diffracted beam; however, the phase angle  $\alpha$  (EQUATIONS 3.3 and 3.4), is not.

$$\alpha = \tan^{-1}(B/A) \quad (3.3)$$

where:

$$F(hkl) = |F(hkl)| e^{i\alpha(hkl)} = A(hkl) + iB(hkl) \quad (3.4)$$

If the following equation:

$$\phi = 2\pi(hx + ky + lz) \quad (3.5)$$

is introduced to the electron density expression (EQUATION 3.2), and after an appropriate mathematical treatment (which has been omitted for simplification purposes, and it is also not the scope of this research), a new electron density expression is obtained as follows:

$$\rho(xyz) = \frac{|F(000)|}{V_c} + \frac{2}{V_c} \sum_{h \geq 0} \sum_k \sum_l |F| \cos(\phi - \alpha) \quad (3.6)$$

all k, l excluding F(000)

NOTE: During the process of mathematical treatment, half of the reflections have been omitted; therefore, a factor of 2 is introduced in EQUATION 3.6.

Therefore, if the  $|F|$  and  $\alpha$ , the phase angle, for each  $h, k, l$ , are known, it is then possible to compute  $\rho$  for all values of  $x, y$ , and  $z$ , and plot the resulting values of  $\rho(xyz)$  to give a three-dimensional electron density map.

Then, assuming atoms to be at the center of peaks, the structure of the crystal can be visualized.

However, since only the structure factor amplitudes  $|F|$  can normally be obtained, and not the phase angles,  $\alpha$ , directly from the experimental measurements, it is therefore necessary to derive  $\alpha$ , either from values of  $|F|\cos(\phi - \alpha)$  that are computed from "trial structures", or by purely analytical methods. The problem of getting estimates of the phase angles so that an image of the scattering matter can be calculated is called the phase problem. The following two sections (3.8 and 3.9) describe the methods used to solve the phase problem, either by deriving a trial structure and so calculating approximate values of  $\alpha$  for each reflection, or by trying to find values of  $\alpha$  directly.

An essential test of the correctness of the model (trial structure) that has been chosen is the fit of the observed structure factor amplitudes to those calculated for the model. The calculations involved, which must eventually be made for all reflections, are impracticable, unless a high-speed computer is available. They generally, however, give a good measure of whether or not the structure is correct. One measure of the correctness of a structure is the so-called discrepancy index or conventional residual,  $R$ , defined as:

$$R = \frac{\sum (||F_o| - |F_c||)}{\sum (|F_o|)} \times 100 \% \quad (3.7)$$

It is a measure of how closely the observed structure factor amplitudes are matched by the values calculated for a proposed trial structure. R values in the range of 2 to 6 % are being quoted for the most reliable determined structures. An R value of 67 % corresponds to a random centrosymmetric structure, that is, with proper scaling, a randomly incorrect structure with a center of symmetry would give an R value of about 67 percent.

If one atom of high atomic number is present in the structure, the initial trial value of R may be much lower because the position of this atom can usually be determined reasonably well even at an early stage, and the heavy atom usually dominates the scattering. If the trial structure is a reasonable approximation to the correct structure, the R value goes down appreciably as refinement proceeds.

However, R is only one measure of the precision (but not necessarily the accuracy) of the derived structure. It denotes how well the calculated model fits the observed data. Many complications can cause errors in the observed or calculated structure factors or both. For example, absorption of the X-rays by the crystal, or atomic scattering factors and temperature factors that do not adequately describe the experimental situation. The fit of the calculated structure factors to the observed ones may then be good, but if the observations are systematically in error, the accuracy of the derived structure may be low, despite an apparently high precision. Hence care must be

taken in interpreting R values. In general, the lower the R value, the better the structure determination, but if one or more very heavy atoms are present, they may dominate the structure factor calculation to such an extent that the contributions from light atoms may not have noticeable effects on R, especially if the structure has not been refined extensively. The positions of the light atoms may then be significantly in error. Also, the resolution of the data (i.e. the maximum value of  $\sin\theta/\lambda$ ) must be taken into account in assessing the meaning of an R value.

### 3.8 The Heavy Atom Method

As the name implies, this method of solving the phase problem involves a heavy atom, which is present in the crystal.

This method follows the tactic as "trial and error", or in simpler words, try to build up a partial structure of the crystal correctly, and then proceed from there onwards. The partial structure which is of interest in this method is certainly the position of the heavy atom (an atom with a high atomic number, Z). For instance, the platinum atom in the structure of  $\text{cis-Pt}(\text{NH}_3)_2\text{Cl}_2$ .

The contribution of any atom to the scattered X-ray intensity is a function of  $Z^2$ , therefore in this case, the majority of intensity is due to the Pt atom, and this contribution will be dominant. Because of this dominance,

it is usually straightforward to find the coordinate of the Pt atom. From EQUATION 3.2, it can be shown that:

$$P(UVW) = \frac{1}{V_C} \sum_{\text{all } h, k, l} |F(hkl)|^2 \exp[2\pi i(hU + kV + lW)] \quad (3.8)$$

This is the expression known as the Patterson function, and a peak occurring at the point  $P(UVW)$ , where  $U$ ,  $V$ , and  $W$  are the coordinate of the point  $P$  on a Patterson vector map results from atoms in the unit-cell at points  $x, y, z$ , and  $x', y', z'$ , where  $U = x - x'$ ,  $V = y - y'$ , and  $W = z - z'$ .

By comparing the coordinate of two identical atoms in adjacent unit-cells, it can be seen that  $x = x'$ ,  $y = y'$ , and  $z = z'$ , which leads to a peak at the origin, where  $U = 0$ ,  $V = 0$ , and  $W = 0$ . Every atom therefore contributes to the origin peak on the Patterson vector map.

The three-dimensional Patterson synthesis provides a vector map of the contents of the unit-cell of the crystal. The value of  $P(UVW)$  will be zero everywhere, except where the values of  $UVW$  represent a vector between two atoms.

In the example given above, the crystal  $\text{cis-Pt}(\text{NH}_3)_2\text{Cl}_2$  has a space group  $P\bar{1}$ . It has two molecules per unit-cell, and the coordinates of the equivalent positions are  $x, y, z$  and  $\bar{x}, \bar{y}, \bar{z}$ . Each molecule in the unit-cell contains a Pt atom. By subtracting the coordinates of equivalent positions, the expected coordinates of the platinum atom-

platinum atom maximum in vector space are found as

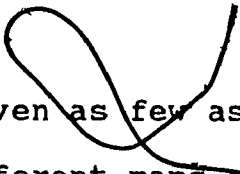
$$U = 2x, V = 2y, \text{ and } W = 2z.$$

### 3.9 The Direct Methods

The "direct methods" concern finding some initial signs directly. Direct methods are usually employed where there are no heavy atoms in the structure, and they differ from the heavy-atom method in being completely objective and dependent solely on mathematical relationships and probabilities. The solution by direct methods can yield either a set of several possible electron density maps, when the most chemically reasonable one is chosen, or alternatively a single result may be obtained which can be right or wrong. Direct methods are relatively more difficult to explain in non-technical terms.

Centrosymmetric structures, with each atom  $x, y, z$ , matched by an equivalent atom in the structure at  $\bar{x}, \bar{y}, \bar{z}$ , are considered first, because the problems presented by non-centrosymmetric structures are more complicated.

In structures with a center of symmetry at the origin, each structure factor has a phase angle either  $0^\circ$  or  $180^\circ$ , so that  $\cos \alpha$  is just  $+1$  or  $-1$ , and  $\sin \alpha = 0$ . Therefore,  $|F| \cos \alpha = F = +|F|$  or  $-|F|$ . However, if  $N$  reflections have been measured for the structure, then a total of  $2^N$  electron density maps are generated, representing all possible combinations of signs for all  $N$  independent structure factors, but only one of these  $2^N$  maps represents the true



density. For even as few as twenty reflections, more than one million different maps can be calculated ( $2^{20} = 1,048,576$ ), and in most cases of structure analysis, more than 1000 reflections are usually recorded. Since the contributions from reflections with high values for the structure factor amplitude will tend to dominate any map calculated, including that calculated with phases corresponding to the correct structure, only the highest valued terms need be considered initially in trying to get an approximation to the correct map. However, even with as few as ten terms, the number of possible maps is 1024, much too high a number to make any simple trial and error method practicable. In the case of a non-centrosymmetric crystal structure, a phase angle may have a value anywhere from  $0^\circ$  to  $360^\circ$ , giving rise to an impossibly large number of maps to work with.

It is possible, however, to derive relations among the phases of different reflections. The relations come from the fact that the electron density can never be negative and is near zero, except for approximately spherical peaks at atomic positions. This implies that the intensities in the X-ray diffraction pattern contain phase information, because the phases are constrained to give positive electron density.

Relationships can be found among the signs of the structure factors and these relationships involve the magnitudes of the larger structure factors normalized in a



certain way, that is, values of the structure factor,  $|F|$ , modified to remove the fall-off in the individual scattering factors,  $f$ , with increasing scattering angle,  $2\theta$ . A normalized structure factor,  $E$ , represents the ratio of a structure factor,  $F$ , to  $(\sum_i f_i)^{1/2}$ , where the sum is taken over all atoms in the unit-cell at the value of  $\sin\theta/\lambda$  appropriate to the  $(h,k,l)$  values for the reflection and includes an overall vibration factor. This sum represents the root-mean-square value that all  $|F|^2$  measurements at the value of  $\sin\theta/\lambda$  would have if the structure were a random one composed of equal atoms. This use of  $F$  values is approximately equivalent to considering each atom to be a point atom.

The exact operation to derive such relationships between the relative phases of certain reflections involves summation of wave functions and will not be presented in this text (See Reference 44).

### 3.10 Least Squares Refinement

Finally, the last step in crystal structure analyses is the least squares refinement, which is a statistical method of obtaining the best fit of a large number of observations to a given equation. This is done by minimizing the sum of the squares of the deviations of the experimentally observed values from their respective calculated ones. The individual terms in the sum are usually weighted to take into account their relative precision. In crystal structure

analyses, atomic coordinates and other parameters may be fitted in this way to the observed intensities; ideally, there should be at least 10 measurements for each parameter to be determined.

The least-squares method, originally described by Legendre (47), proceeds by making the sum of the squares of the errors in  $F_0$  a minimum. An iterative process is carried out and after each cycle an improved value for each parameter is obtained. The procedure is repeated until no further improvement takes place, as shown by the so-called discrepancy index or conventional residual,  $R$  (EQUATION 3.7).

#### 4.0 $^{119}\text{Sn}$ TIN MÖSSBAUER SPECTROSCOPY AND ELECTRICAL PROPERTIES OF STANNOUS HALIDES

##### 4.1 Resonant Absorption and Fluorescence

The recoilless nuclear resonant emission and absorption (or fluorescence) of  $\gamma$ -rays is more commonly known as the Mössbauer effect, and is used as a spectroscopic technique (Mössbauer spectroscopy).

Atomic resonant fluorescence was predicted and discovered just after the turn of the century, and within a few years, the underlying theory had been developed. From a simplified viewpoint, an atom in an excited electronic state can decay to its ground state by the emission of a photon to carry off the excess energy. This photon can then be absorbed by a second atom of the same kind by electronic excitation. Subsequent de-excitation re-emits the photon, but not necessarily in the initial direction, so that scattering or resonant fluorescence occurs. So if the monochromatic yellow light from a sodium lamp is collimated and passed through a glass vessel containing sodium vapour, one would expect to see a yellow glow as the incident beam is scattered by resonant fluorescence.

A close parallel can be drawn between atomic and nuclear resonant absorption. The primary decay of the majority of radioactive nuclides produces a daughter nucleus which is in a highly excited state. The latter then de-excites by emitting a series of  $\gamma$ -ray photons until, by one or more routes, depending on the complexity of the

$\gamma$ -cascade, it reaches a stable ground state. This is clearly analogous to electronic de-excitation, the main difference being in the much higher energies involved in nuclear transitions.

It was believed that, according to theory, it should be possible to use the  $\gamma$ -ray emitted during a transition to a nuclear ground-state to excite a second stable nucleus of the same isotope, as to give rise to nuclear resonant absorption and fluorescence. However, experiments to detect these processes at early stages were not successful because of the nuclear recoil and Doppler broadening (thermal energy) effects.

It can be shown, from fundamental physics, that when a nucleus is considered isolated and has an excited state energy, the  $\gamma$ -ray energy emitted differs from the energy of the nuclear transition by the nuclear recoil kinetic energy (line shift) and is spread over a wide energy range by the Doppler energy line broadening, which is a thermal energy. For nuclear resonant absorption to occur at a significant level, the emission and absorption energy distributions have to have a strong overlap region, but the recoil and Doppler energy clearly prevent this.

#### 4.2 The Mössbauer Effect

From the above analogy, it can be seen how the recoil energy and the Doppler effect, for a nucleus at an isolated state, with an excited nuclear state energy, preclude the nuclear resonant absorption process.

The Mössbauer effect is unique in that it provides a means of eliminating the destructive effects of the recoil and thermal energies. The key to the problem lies in the behaviour of the recoiling nucleus when it is no longer isolated (as is the former case), but instead is fixed in a solid lattice, crystalline or not. The recoil energy is much less than the chemical binding energy, but is similar in magnitude to the lattice-vibration phonon energies. If the recoil energy is transferred directly to vibrational energy, then the  $\gamma$ -ray energy is still degraded. However, the phonon energies are quantized, and the recoil energy can only be transferred to the lattice if it corresponds closely to an allowed quantum jump.

The simplest mathematical treatment is one in which the vibrational characteristics correspond to an Einstein solid with one vibrational frequency,  $\omega$ . Transfer of energy to the lattice can only take place in integral multiples of  $\hbar\omega$  ( $0, \pm \hbar\omega, \pm 2\hbar\omega$ , etc., where  $\hbar$ , Planck's constant,  $= 2\pi\hbar$ ). If the recoil energy  $E_R$  is less than  $\hbar\omega$ , then either zero or one unit of  $\hbar\omega$  of vibration energy may be transferred to the lattice (48,49). It has been demonstrated that when many emission processes are considered, the average energy transferred per event must exactly equal  $E_R$  (50). From the analogy in the previous section, it is the mass of an isolated nucleus being considered; however, the mass involved in this section is increased to that of a crystallite containing an average of  $10^{15}$  atoms, hence both

the recoil energy and the Doppler broadening become very small.

In an absorption Mössbauer spectroscopic experiment (See FIGURE 4.1), recoilless  $\gamma$ -rays emitted by a radioactive source are sent through a thin absorber, which is the sample, and the radiation transmitted by the sample is recorded, as a function of the  $\gamma$ -ray energy.

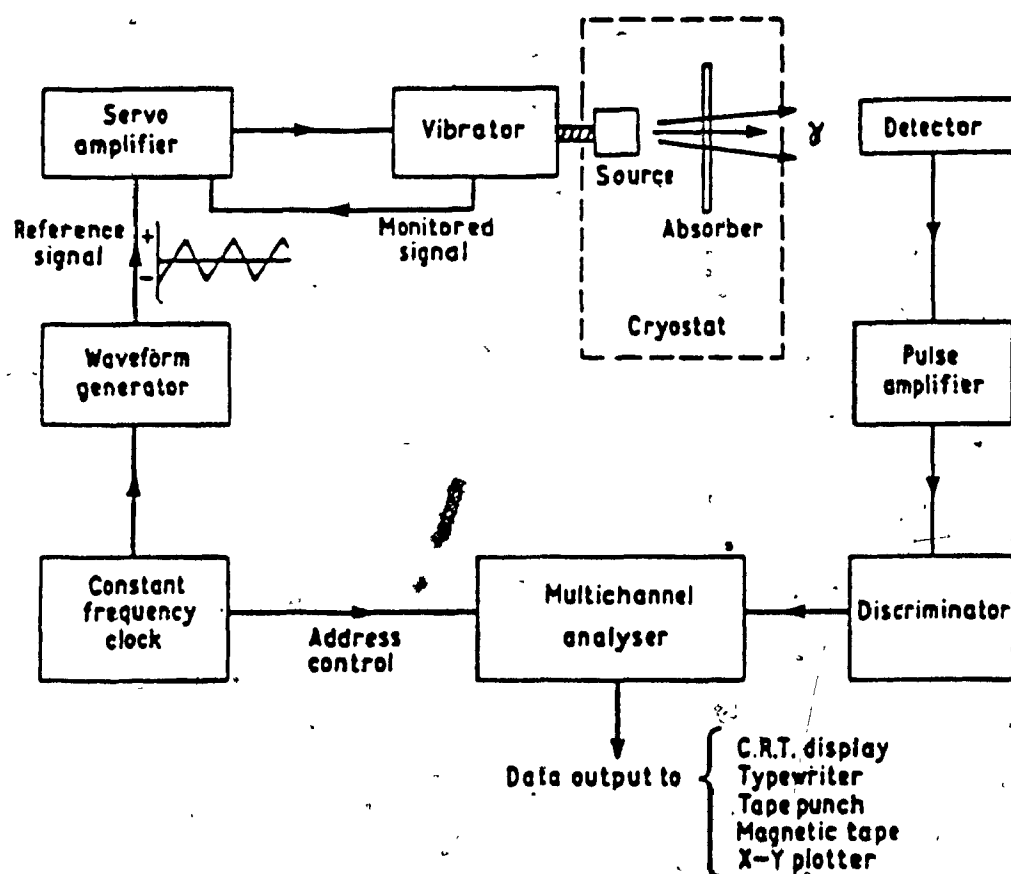


FIGURE 4.1 Schematic diagram for a Mössbauer experimental set-up.

The energy of the  $\gamma$ -rays is modulated by Doppler effect upon moving the source relative to the absorber. Only the

fraction  $f_a$  of nuclei in the sample absorbs the  $\gamma$ -photon resonantly, i.e. without recoil, hence giving rise to a Mössbauer spectrum. The fraction  $f_a$  is called "recoil-free fraction" or "recoilless fraction". The fraction  $(1 - f_a)$  dissipates the recoil energy in the form of phonons. As nuclear energy levels are quantized, the energy of a  $\gamma$ -photon absorbed by a nucleus gives the difference of energy between the ground and first excited states. These energy levels shift when subjected to an electric monopole and split when an electric field gradient and/or a magnetic field act at the nucleus.

These interactions, known as the "Hyperfine Interactions", result in shifts and splitting of the Mössbauer absorption lines, making possible a study of the electric and magnetic phenomena which cause them.

#### 4.3 Hyperfine Interactions

There are three principal interactions to consider. However, only two are of particular interest to this research and they are as follows:

- a) Electric monopole interaction. It results from a change in the electric monopole (or coulombic) interaction between the electronic and nuclear charges, which is caused by a difference in the size of the nucleus in its ground and excited states. It is proportional to the s electron density at the nucleus and gives rise to a line shift called "chemical isomer shift" or simply

"isomer shift", which has the symbol  $\delta$  (FIGURE 4.2a).

It is a good probe for changes in bonding, in electron distribution, oxidation state and electron withdrawing power of the ligands.

b) Electric quadrupole interaction. It occurs between the nuclear quadrupole moment and the local electric field gradient tensor at the nucleus, and only those nuclear states with spin  $I$  greater than  $1/2$  have a nuclear quadrupole moment and hence show a quadrupole hyperfine splitting. The effect of this interaction is proportional to the electric field gradient (e.f.g.) at the nucleus, and the e.f.g. can have two origins:

- (e.f.g.)<sub>val</sub>: valence contribution due to uneven filling of non-spherical orbitals (p,d,f).
- (e.f.g.)<sub>lat</sub>: lattice contribution due to a non-regular coordination (i.e. other than cubic, tetrahedral or octahedral).

In the case of  $^{119}\text{Sn}$ , the transition involved between the nuclear spin states is  $1/2 \rightarrow 3/2$ ; a non-zero e.f.g. gives rise to two lines and the spacing between them is called "quadrupole splitting", symbolized as  $\Delta$  (FIGURE 4.2b).

Therefore, a measure of the isomer shift and quadrupole splitting for  $^{119}\text{Sn}$  allows probing for the tin electrical environment, which influences the conduction properties as explained in Paragraph 4.4. In addition, the recoil-free



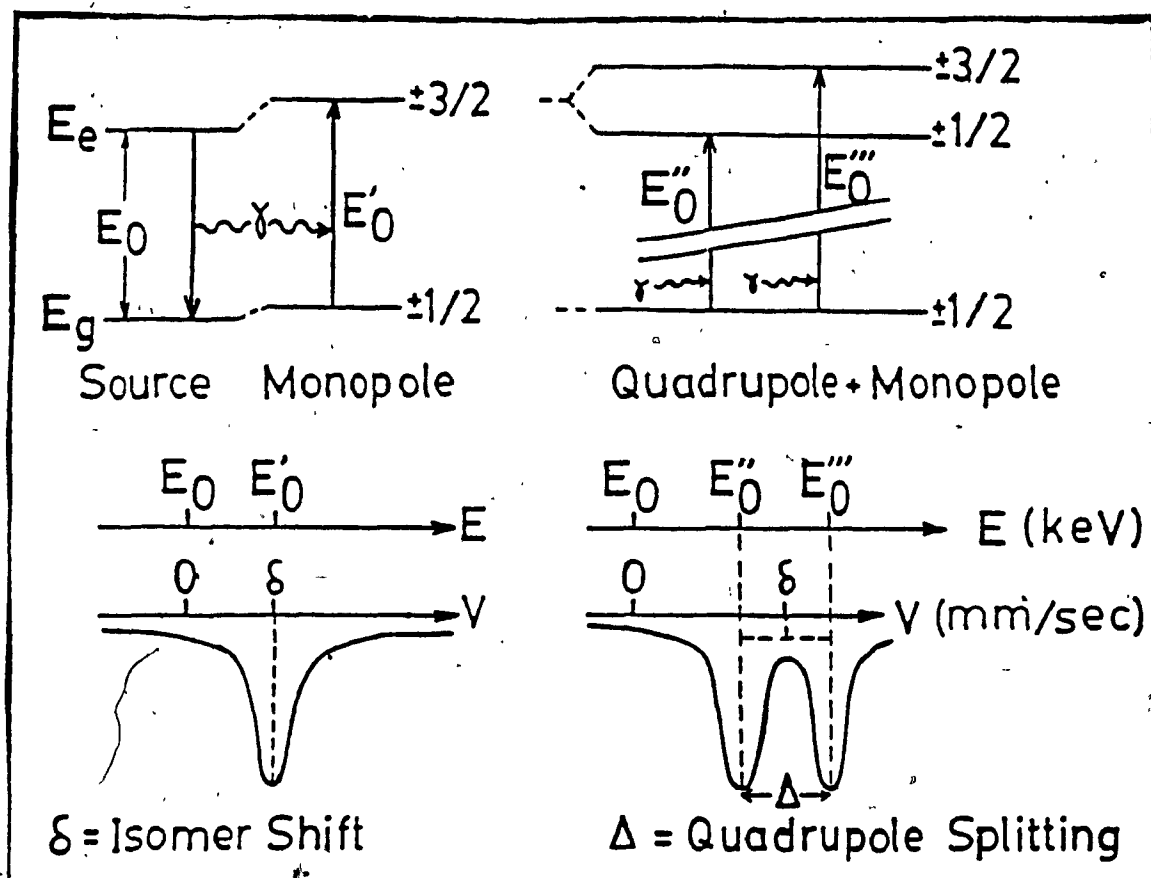


FIGURE 4.2 (a and b) Mössbauer hyperfine interactions of:  
 (a) electric monopole; (b) electric quadrupole.

fraction depends on the lattice strength and thus allows a study of the dynamic properties of the material. As scanning the  $\gamma$ -ray energy is done by Doppler effect, upon moving the  $\gamma$ -ray source relative to the absorber, the line positions are given in velocity units (mm per sec) instead of energy units. This is more convenient in a sense that line shifts and splittings are very small compared to the  $\gamma$ -ray energy.

#### 4.4 Electrical Properties of Divalent Tin Halides

Divalent tin halide materials have been found to exhibit a variety of electric conductivity mechanisms; for instance, ionic (for fluorides), semiconducting, and metallic (bromides and iodides). In ionic conductors, the charge carriers are ions which can undergo long distance translational motion when the sample is placed in an electric field. Long distance ion motion in solids can take place according to several processes depending on the crystal structure: (i) in empty spaces of the structural networks (empty planes in  $\beta$ -aluminas), (ii) via ionic sites with an occupancy factor much lower than unity ( $\beta$ -AgI, for example), or (iii) or via lattice defects (Frenkel defects in the fluorite-type structure). Semiconduction is observed when the band gap in solids is low enough ( $\leq 2$  eV) to allow thermal or photoexcitation of electrons from the filled valance band to the empty conduction band. Metal-type conduction occurs when the valence band is not totally

filled, allowing easy electron mobility. The electrical properties of tin-containing materials can be correlated to the tin electronic structure and coordination, which allows easy and fast investigation of the potential electrical properties just using Mössbauer spectroscopy. Typical Mössbauer spectra characteristic of each type of electrical properties are shown on FIGURE 4.3. Spectrum 4.3a is that of  $\text{CaSnO}_3$  (tin(IV): electronic structure is  $5s^0 5p^0$ ), which is the isomer shift reference, therefore its line position is taken as  $\delta = 0$ . Its quadrupole splitting is also equal to zero as there is no 5p electron around tin, i.e. (e.f.g.)<sub>val</sub> = 0, and the structure is cubic, of perovskite-type with a regular octahedral environment of tin, and as a consequence (e.f.g.)<sub>lat</sub> = 0. Divalent tin has a  $5s^{2-x} 5p^x$  or  $5s^{2-x-y} 5p^x 5d^y$  (depending on the type of hybridization) electronic structure, therefore the (2-x) [or (2-x-y)] s electrons surrounding tin give a high isomer shift to tin(II) compounds. In fluorides, a value of  $\delta$  about 3.5 mm per sec is usually observed (FIGURE 4.3b). In the fluorides, tin(II) has two non-bonding electrons ( $5s^{2-x} 5p^x$  or  $5s^{2-x-y} 5p^x 5d^y$ ), which are located on a non-bonding orbital. However, this orbital is neither a pure s nor a pure p or d orbital. It is one of the following hybridized molecular orbitals:  $sp^3$ ,  $sp^3d$ , or  $sp^3d^2$ , depending on the tin coordination. As one of these orbitals contains the  $5s^{2-x} 5p^x$  (or  $5s^{2-x-y} 5p^x 5d^y$ ) non-bonding electron pair, a very irregular coordination is observed. A  $sp^3$

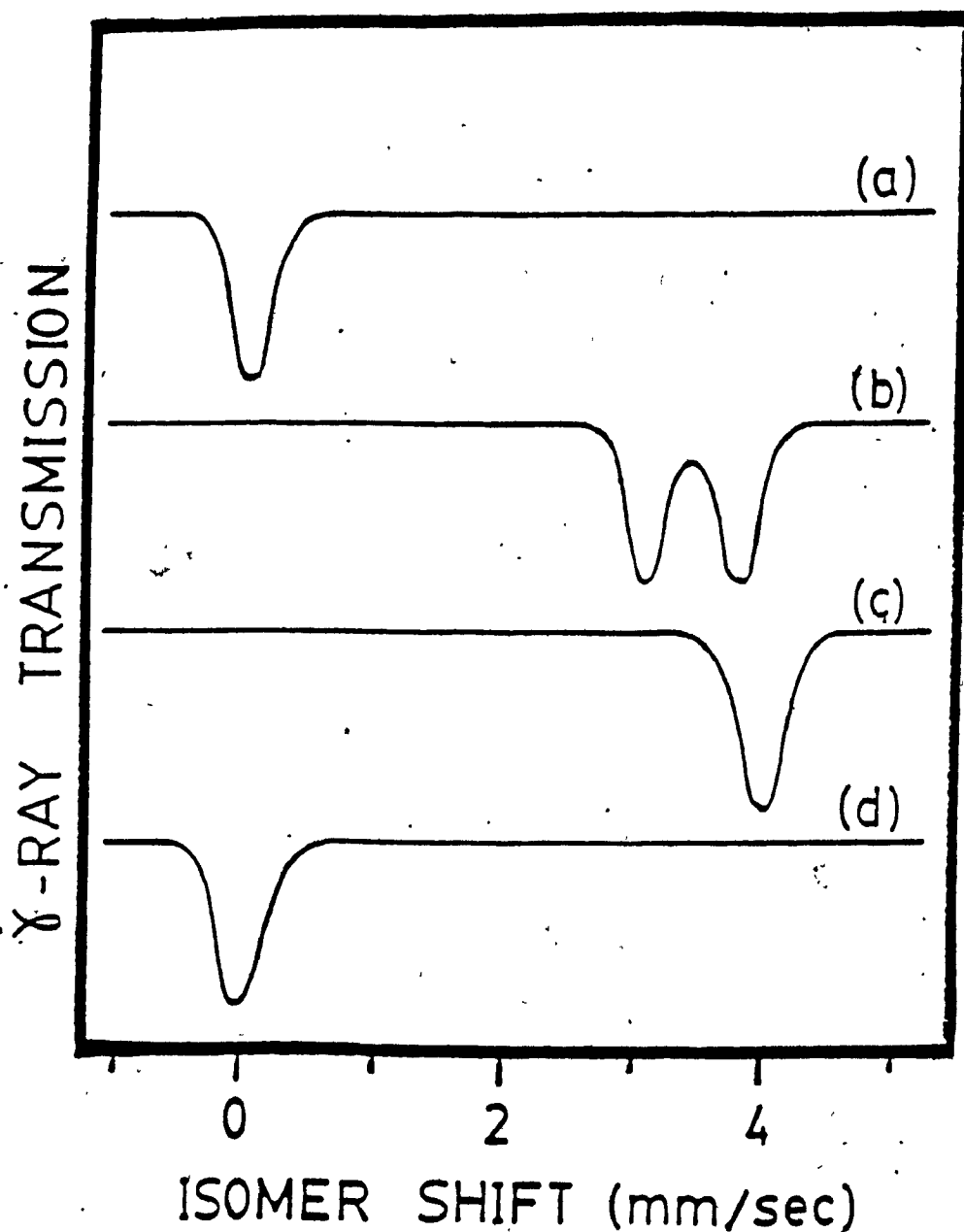


FIGURE 4.3 (a  $\rightarrow$  d)  $^{119}\text{Mössbauer}$  spectra of tin(II) halide compounds, as a function of their electrical properties: (a)  $\text{CaSnO}_3$  reference ( $\delta = 0$ ,  $\Delta = 0$ ); (b) ionic conductor or insulator fluorides ( $\delta \approx 3.5$ ,  $\Delta \approx 1.5$ ); (c) bromide or iodide semiconductor ( $\delta \approx 4.0$ ,  $\Delta \approx 0$ ); (d)  $\text{CsSnBr}_3$ ,  $T > 418$  K, metal-type conductor ( $\delta \approx 0$ ,  $\Delta \approx 0$ ).

hybridization gives a  $\text{SnX}_3\text{E}$  pseudotetrahedral environment,  $\text{sp}^3\text{d}$  a  $\text{SnX}_4\text{E}$  pseudotrigonal bipyramid, and  $\text{sp}^3\text{d}^2$  a  $\text{SnX}_5\text{E}$  pseudooctahedral coordination, where E represents the lone pair, which occupies one of the apexes of the tin polyhedron of coordination (33). This has two major following consequences:

- (a) Such a lone pair is located in a localized orbital, which does not extend beyond the tin atom it belongs to. Therefore, these two electrons, even though they are not used for bonding, are not mobile and cannot give rise to any type of electronic conductivity.
- (b) The lone pair is in a  $5\text{s}^{2-x}5\text{p}^x$  (or  $5\text{s}^{2-x-y}5\text{p}^x5\text{d}^y$ ) hybridized orbital. The p (and d) contribution to the lone pair creates a large electric field gradient, which gives rise to a large quadrupole splitting, most of which originates from  $(\text{e.f.g.})_{\text{val}}$ . The distorted environment around tin also gives a non-zero  $(\text{e.f.g.})_{\text{lat}}$ ; however, this is usually a minor component and can be totally masked by the much larger  $(\text{e.f.g.})_{\text{val}}$ . For large alkali metals (Cs) and for low electronegativity halides (Br, I), the amount of p electrons in the lone pair decreases, and consequently the amount of s electrons increases and it results in a higher isomer shift and smaller quadrupole splitting. In some cases, such as the  $\text{CsMX}_3$  ( $\text{X} = \text{Cl}, \text{Br}, \text{and I}$ ) compounds, the structure is of perovskite-type, i.e. tin(II) is in a regular octahedral site. Such a

coordination cannot be achieved if there is any p electron density in the tin non-bonding pair; therefore, in these compounds, the lone pair is pure s (therefore, of spherical shape), i.e. the tin(II) electronic structure is  $5s^2 5p^0$ . It results in a higher isomer shift (about 4.00 mm per sec) and zero quadrupole splitting as both  $(e.f.g.)_{val}$  and  $(e.f.g.)_{lat}$  are equal to zero (FIGURE 4.3c) (31). In some rare cases, such as  $CsSnBr_3$ , upon heating, at 418 K, an electrical phase transition occurs, from semiconduction to metal-type conduction (14). At the same time, the Mössbauer spectrum changes from the type (c) to the type (d) of FIGURE 4.3. Such a behaviour indicates that the tin lone pair of electrons is transferred from the localized  $5s^2$  orbital to a conduction band, giving rise to metal type conduction (14). In addition, as these electrons are on a band which extends over the whole crystal, they are no longer around each individual tin atom. As a result, there is a drastic decrease in s electron density around tin, which, having lost two electrons to populate the conduction band, behaves like tetravalent tin, and the Mössbauer spectrum obtained is a tin(IV) spectrum (FIGURE 4.3d) identical to that of the isostructural  $CaSnO_3$  perovskite-type structure (FIGURE 4.3a). In the present study, the conductivity properties of the materials isolated were not measured. However, they

were one of the driving forces of the project and some evaluation of potential conducting properties has been performed, based on the structural and Mössbauer results, which provide important information on the electronic structure of divalent tin.

## 5.0 EXPERIMENTAL RESULTS

### 5.1 Products Obtained from Reactions

The reactions between  $\text{SnF}_2$  and  $\text{MCl}$  ( $\text{M} = \text{NH}_4$ ,  $\text{K}$ , and  $\text{Na}$ ) were carried out at different ratios listed as follows:

- (a)  $\text{SnF}_2 + \text{MCl}$
- (b)  $\text{SnF}_2 + 2 \text{MCl}$
- (c)  $\text{SnF}_2 + 5 \text{MCl}$
- (d)  $\text{SnF}_2 + 10 \text{MCl}$
- (e)  $2 \text{SnF}_2 + \text{MCl}$
- (f)  $5 \text{SnF}_2 + \text{MCl}$
- (g)  $10 \text{SnF}_2 + \text{MCl}$

When the initial molar ratio of one of the starting reagents was high, such as in reactions c, d, f, and g, the reagent in large excess ( $\text{MCl}$  or  $\text{SnF}_2$ ), was obtained as major product.

When ratios between the two starting materials were about 1:1 (i.e. reactions a, b, and e), new compounds were obtained except in the case where  $\text{M} = \text{Na}$ . Sodium pentafluorodistannate(II),  $\text{NaSn}_2\text{F}_5$ , which has already been identified and studied (16,20), was the product obtained from such reactions.

Other known compounds, such as potassium pentafluorodistannate(II),  $\text{KSn}_2\text{F}_5$  (16,21) and tri-fluorochloroditin,  $\text{Sn}_2\text{F}_3\text{Cl}$  (51) were also obtained as by-products in certain reactions. These two compounds have both been identified by earlier researchers and their crystal structures have as well been solved (52).



New compounds from this research have been identified. They are  $(\text{NH}_4)_3\text{Sn}_5\text{F}_{10}\text{Cl}_3$  and  $\text{K}_3\text{Sn}_5\text{F}_{10}\text{Cl}_3$ , respectively. However, various evidence suggested that the former compound does not represent the batch of crystals collected with such stoichiometry. That is to say, other ammonium-tin-halo complexes, of the type  $(\text{NH}_4)_u\text{Sn}_v\text{F}_x\text{Cl}_y$  (with  $u + 2v = x + y$ ), have also been observed, and their exact stoichiometries have yet to be determined. Thus far, three different ammonium chloride-tin-fluoride complexes from this research have been studied and one of which has been confirmed to have the above mentioned molecular formula. This particular species was chosen for X-ray structure analysis. The details of which are presented in Chapter Six. However, chemical analyses suggested that the average chemical composition of the batch is intermediate between  $\text{NH}_4\text{Sn}_2\text{F}_4\text{Cl}$  and  $(\text{NH}_4)_3\text{Sn}_5\text{F}_{10}\text{Cl}_3$ . The coexistence of several ammonium-tin-halo complexes was easily demonstrated by X-ray film diffraction studies, since three single crystals were chosen for that purpose and each of them gave different symmetry elements and space groups. The three species give needle-shaped colourless crystals which cannot be distinguished by simple visual inspection.

On the other hand, this problem was never observed in the potassium case. This was also proven by X-ray film diffraction studies (oscillation, Weissenberg, precession and Laue methods) of several single crystals, and they all gave the same symmetry elements and unit-cell parameters.

In addition to that, the X-ray powder diffraction pattern of the batch was fully indexable using the information obtained from the film diffraction studies (i.e. Weissenberg and precession), suggesting that the batch of crystals was indeed in a homogeneous phase. Otherwise, indexation as a single phase would not have been possible.

The physical appearance of the new compounds from both cases are shown in FIGURE 5.1.

## 5.2 Crystallographic Data for the New Compounds from the $\text{NH}_4\text{Cl}/\text{SnF}_2$ System

The reactions between  $\text{NH}_4\text{Cl}$  and  $\text{SnF}_2$  at about 1:1 ratio give rise to various ammonium-tin-halo complexes of the type  $(\text{NH}_4)_u\text{Sn}_v\text{F}_x\text{Cl}_y$ . Three of them have been studied in terms of symmetry elements and space groups determination, and they are listed as below:

### (a) Compound A = $[(\text{NH}_4)_3\text{Sn}_5\text{F}_{10}\text{Cl}_3]$

NOTE: This was the one chosen for structure analysis  
(See Chapter Six).

- Unit-Cell Parameters:  $a = 4.401 \text{ \AA}$   
 $b = 20.999 \text{ \AA}$   
 $c = 19.794 \text{ \AA}$   
 $\alpha = \beta = \gamma = 90^\circ$
- Crystal System: Orthorhombic
- Confirmed Space Group: Bmmb (Number 63, standard Cmc<sub>2</sub>m)

a.)



b.)

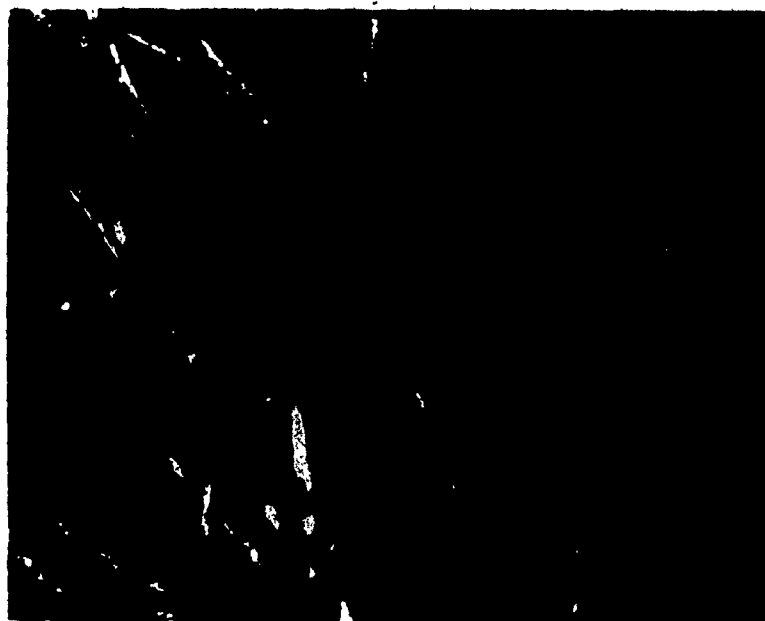


FIGURE 5.1 The physical appearance of: (a)  $\text{NH}_4\text{Sn}_2\text{F}_4\text{Cl}/(\text{NH}_4)_3\text{Sn}_5\text{F}_{10}\text{Cl}_3$ ; (b)  $\text{K}_3\text{Sn}_5\text{F}_{10}\text{Cl}_3$ .

(b) Compound B

- Unit-Cell Parameters:  $a = 4.341 \text{ \AA}$   
 $b = 20.257 \text{ \AA}$   
 $c = 15.193 \text{ \AA}$   
 $\alpha = \beta = \gamma = 90^\circ$
- Crystal System: Orthorhombic
- Possible Space Groups:  $P2_1mn$  (Number 31)  
 $Pmmn$  (Number 59)

(c) Complex C

- Unit-Cell Parameters:  $a = 4.947 \text{ \AA}$   
 $b = 9.248 \text{ \AA}$   
 $c = 6.861 \text{ \AA}$   
 $\alpha = \gamma = 90^\circ, \beta = 92.25^\circ$
- Crystal System: Monoclinic
- Possible Space Groups:  $P2_1$  (Number 4)  
 $P2_1/m$  (Number 11)

The X-ray powder diffraction pattern was not indexable, since the batch of crystals was a mixture of different species.

5.3 Crystallographic Data for the New Compound from the KCl/SnF<sub>2</sub> System

The new compound,  $K_3Sn_5F_{10}Cl_3$ , from this system is not as complicated as in the ammonium case. This complex only crystallizes out in a single phase, and the crystallographic data are as follows:

- Unit-Cell Parameters:
  - $a = 4.358 \text{ \AA}$
  - $b = 20.246 \text{ \AA}$
  - $c = 19.204 \text{ \AA}$
  - $\alpha = \beta = \gamma = 90^\circ$
- Crystal System: Orthorhombic
- Number of repeating units in the unit-cell:  $Z = 4$
- Possible Space Groups:
  - $Bm2_1b$  (Number 36, standard  $Cmc2_1$ )
  - $B2mb$  (Number 40, standard  $Ama2$ )
  - $Bmmb$  (Number 63, standard  $Cmcm$ )

The X-ray powder diffraction pattern is summarized in TABLE 5.1.

#### 5.4 Chemical Analytical Results

(a) The chemical composition for the new materials from the  $NH_4Cl/SnF_2$  system:

	<u>NH<sub>4</sub></u>	<u>Sn</u>	<u>F</u>	<u>Cl</u>
Theoretical values for $NH_4Sn_2F_4Cl$	4.90 %	64.83 %	20.71 %	9.66 %
Theoretical values for $(NH_4)_3Sn_5F_{10}Cl_3$	5.72 %	62.88 %	20.13 %	11.27 %
Experimental values	4.91 %	60.54 %	19.12 %	10.99 %

The experimental values are indications for the batch of crystals to have a stoichiometry close to  $NH_4Sn_2F_4Cl$  and

$h$	$k$	$l$	$I/I_0$	$d_m$ (Å)	$d_c$ (Å)
0	0	2	7	9.571	9.602
0	0	4	35	4.801	4.801
1	2	1	4	3.931	3.921
1	1	3	8	3.534	3.547
1	2	3	12	3.391	{ 3.396
0	6	0			{ 3.391
0	0	6	65	3.191	{ 3.201
0	6	2			{ 3.197
1	3	3	100	3.160	3.181
0	2	6	27	3.056	3.053
1	4	3	7	2.967	2.940
0	4	6	4	2.730	2.709
0	8	0	5	2.536	2.543
1	4	5	3	2.505	2.507
0	8	2	3	2.438	2.458
0	0	8	6	2.390	{ 2.400
1	7	1			{ 2.399
1	5	5	2	2.356	2.352
1	3	7	6	2.214	2.197
2	0	0	12	2.179	2.179
2	0	2	2	2.118	{ 2.125
2	1	2			{ 2.113
0	10	0	4	2.040	2.035
1	9	1	2	1.9935	{ 1.9958
0	8	6			{ 1.9912
1	9	3	20	1.9118	1.9148
0	2	10			{ 1.8871
2	5	2	2	1.8842	{ 1.8835
1	2	9			{ 1.8833
2	4	4	6	1.8504	1.8485
2	0	6	7	1.8025	{ 1.8011
2	6	2			{ 1.8006
2	2	6	3	1.7693	1.7736
0	8	8	5	1.7442	1.7457
0	6	10	4	1.6800	1.6710
0	2	12	14	1.5821	1.5809
2	9	2	2	1.5461	{ 1.5483
1	4	11			{ 1.5441
0	8	10	6	1.5316	{ 1.5326
2	7	6			{ 1.5310

TABLE 5.1 Indexed X-ray powder pattern of  $K_3Sn_5F_{10}Cl_3$ .

$(\text{NH}_4)_3\text{Sn}_5\text{F}_{10}\text{Cl}_3$ . They certainly implied the co-existence of several species within the batch in a sense (as shown by X-ray film diffraction studies).

(b) The chemical composition determined for the new material from the  $\text{KCl}/\text{SnF}_2$  system is close to the theoretical values for  $\text{K}_3\text{Sn}_5\text{F}_{10}\text{Cl}_3$ :

	<u>K</u>	<u>Sn</u>	<u>F</u>	<u>Cl</u>
Theoretical values for $\text{K}_3\text{Sn}_5\text{F}_{10}\text{Cl}_3$	11.65 %	58.93 %	18.86 %	10.56 %
Experimental values	9.52 %	56.74 %	17.92 %	10.82 %

#### 5.5 Summary of Mössbauer Experiments

The Mössbauer spectra for the new materials, both in crystal and powder form, are shown in FIGURE 5.2. All spectra have the same doublet, similar to that of  $\alpha\text{-SnF}_2$ , which is given as a reference. The doublet observed is a characteristic of the  $5s^{2-}5p^x$  electron lone pair of tin(II). The Mössbauer parameter for the materials are summarized, along with that from other related compounds (for comparison purposes), in TABLE 5.2.

#### 5.6 Thermal Gravimetric Analyses

The results obtained from thermal gravimetric analyses for the new materials from both systems are shown in FIGURE 5.3.

The thermogram (FIGURE 5.3a) for the potassium complex confirmed that there was not any water of crystallization in

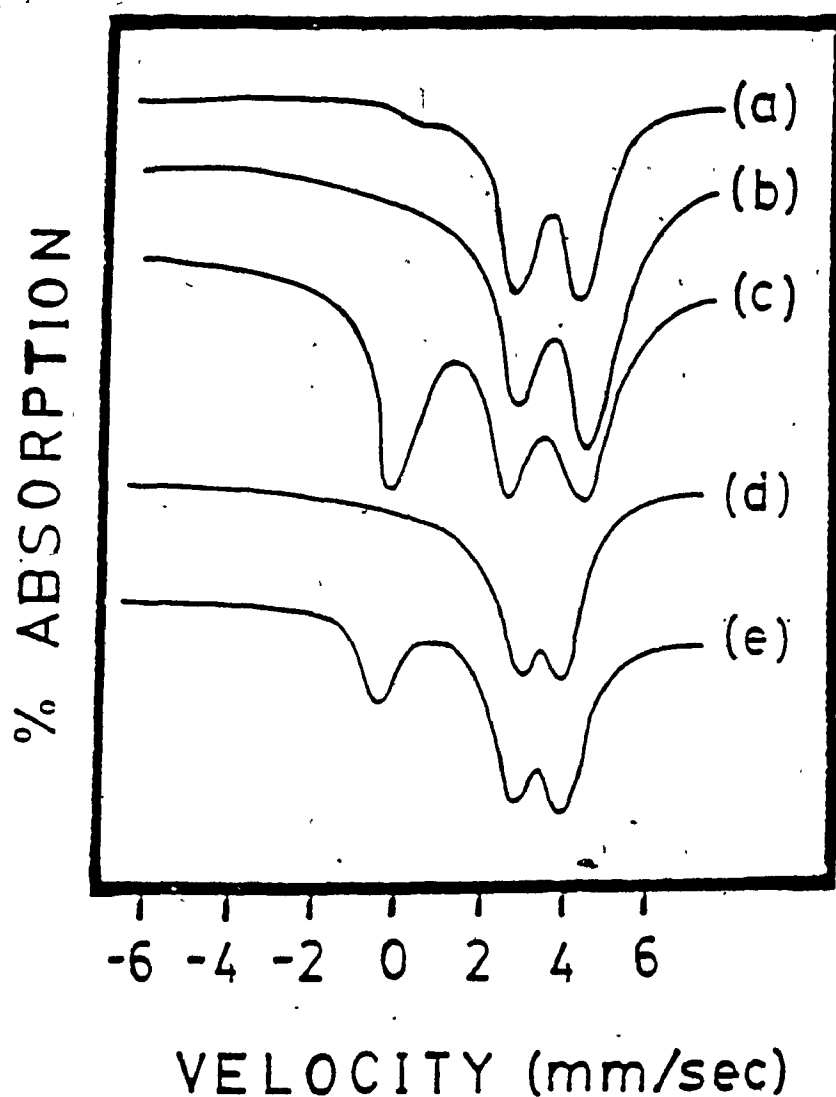


FIGURE 5.2  $^{119}\text{Sn}$  Mössbauer spectra of the new products from  $\text{MCl}/\text{SnF}_2$ , ( $\text{M} = \text{K}, \text{NH}_4$ ). The spectrum of  $\alpha\text{-SnF}_2$  is given for comparison. (a)  $\alpha\text{-SnF}_2$ ; (b)  $\text{K}_3\text{Sn}_5\text{F}_{10}\text{Cl}_3$  (collection of crystals); (c)  $\text{K}_3\text{Sn}_5\text{F}_{10}\text{Cl}_3$  (powder, after grinding); (d)  $\text{NH}_4\text{Sn}_2\text{F}_4\text{Cl}/(\text{NH}_4)_3\text{Sn}_5\text{F}_{10}\text{Cl}_3$  (collection of crystals); (e)  $\text{NH}_4\text{Sn}_2\text{F}_4\text{Cl}/(\text{NH}_4)_3\text{Sn}_5\text{F}_{10}\text{Cl}_3$  (powder, after grinding).



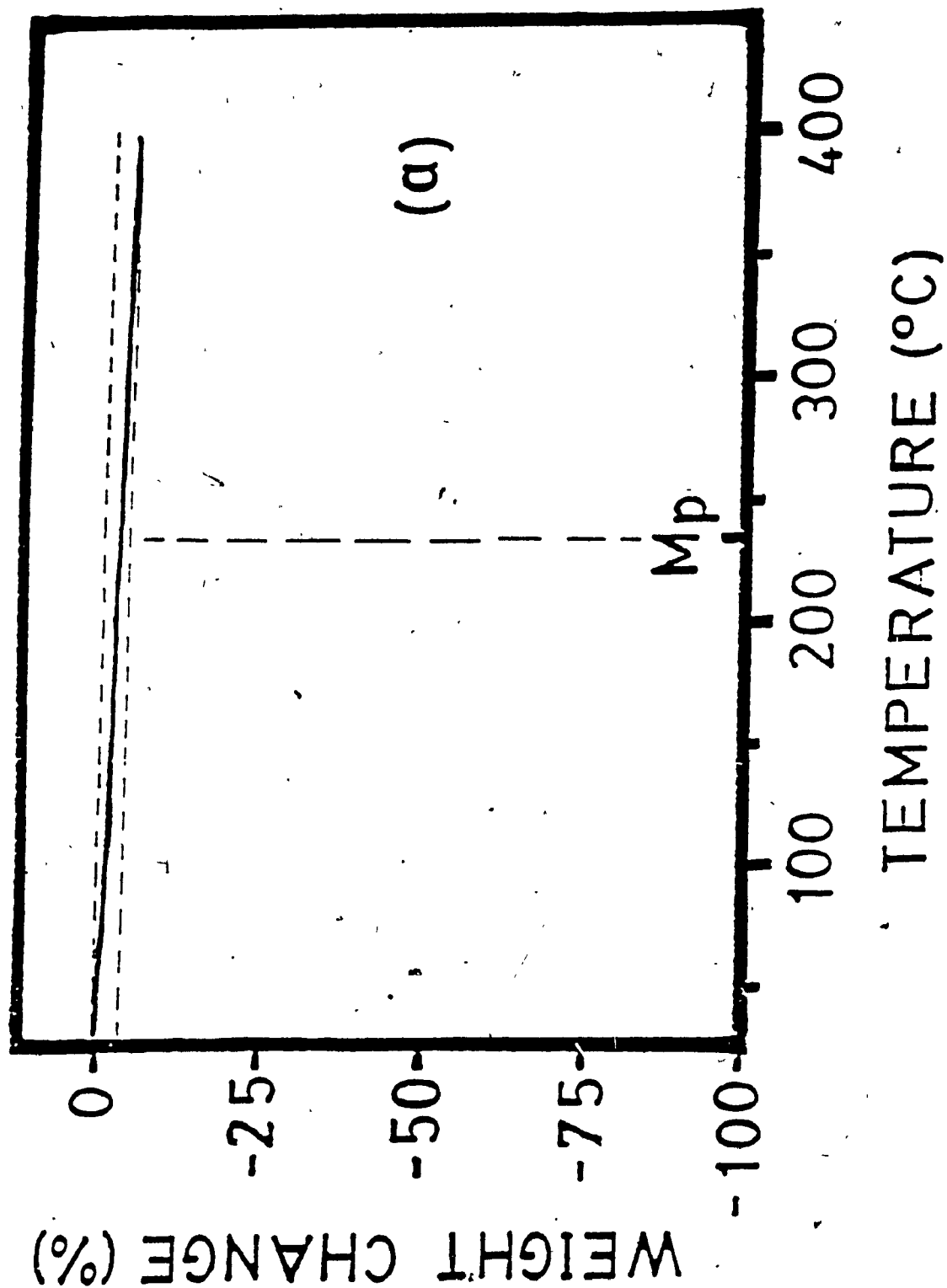


FIGURE 5.3 The thermogram of: (a)  $\text{K}_3\text{Sn}_5\text{F}_{10}\text{Cl}_3$ ; (b)  $\text{NH}_4\text{Sn}_2\text{F}_4\text{Cl}/(\text{NH}_4)_3\text{Sn}_5\text{F}_{10}\text{Cl}_3$ .

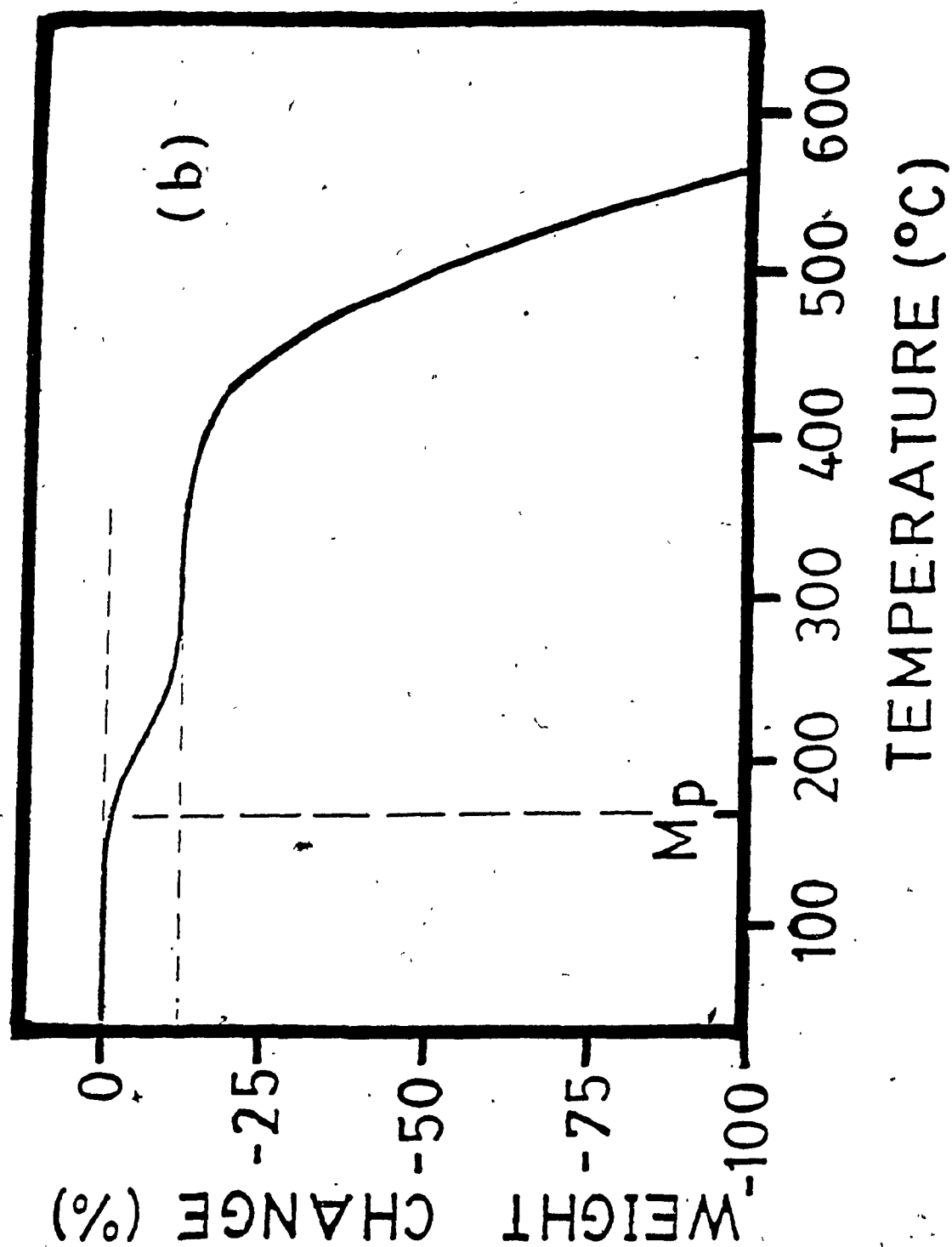


FIGURE 5.3 - cont'd

**TABLE 5.2**  
Mössbauer spectroscopic parameters for materials obtained from this research and other related compounds.

<u>Compound</u>	<u>Colour</u>	$\delta$ (a,b) (mm/sec)	$\Delta$ (a) (mm/sec)	<u>References</u>
$K_3Sn_5F_{10}Cl_3$	White	3.38	1.47	This Work
$NH_4Sn_2F_4Cl / (NH_4)_3Sn_5F_{10}Cl_3$	White	3.50	1.12	This Work
$\alpha-SnF_2$	White	3.43	1.53	55
$KSn_2F_4I$	Yellow	3.33	1.84	32
$KSnF_2I$	Orange	3.37 3.82	1.75 0.00	32
$KSn_3F_6I$	Yellow	3.66	0.00	32
$KSn_2F_5$	White	3.21	1.96	56
$NH_4Sn_2F_4I$	Yellow	3.48	1.48	32
$NH_4SnF_2I$	Orange	3.45 3.92	1.68 0.00	32
$NH_4Sn_3F_6I$	Yellow	3.39	1.58	32
$NH_4Sn_2F_5$	White	3.28	1.94	56
$CsSnF_3$	Grey	2.93	1.86	31
$CsSnF_2I$	Brown	2.96	1.82	31
$CsSnBr_3$	Black	3.93	0.00	31
$CsSnCl_3$	Yellow	3.70	ca. 0	31

(a)  $\pm 0.01 \text{ mm.s}^{-1}$ .

(b) Relative to  $CaSnO_3$  at room temperature.

the species. The slight decrease of weight observed with temperature rise was most likely due to hydrolysis of a part of the sample due to the presence of traces of moisture in

the nitrogen atmosphere, as evidenced by black SnO residue with HF being evolved according to Reaction 5.1.



Complete hydrolysis for the above reaction would correspond to a weight loss of about 12 %. However, as the measured weight loss was less than 2 %, we can conclude that less than 17 % of the sample was hydrolyzed.

The reactivity of tin(II) halide containing compounds to hydrolysis is thermally activated and increase drastically at melting. As a constant weight loss is observed above ca. 80 °C, and no visible change occurs at melting, it can be concluded that the kinetics of hydrolysis is determined by the amount of water available, i.e. by the concentration of water in nitrogen and by the nitrogen flow rate.

The TGA curve for the ammonium case is very different (FIGURE 5.3b) from that of the potassium. It shows a weight loss starting at about 140 °C, and then accelerates to give a total of about 12 % decrease at 320 °C, where a plateau is seen. This can be interpreted as being the decomposition of the sample, with loss of  $\text{NH}_4\text{F}$ ,  $\text{NH}_4\text{Cl}$ , or a mixture of both, according to the following proposed reactions (recall from Section 5.4, the average chemical composition for the batch of crystals is between  $\text{NH}_4\text{Sn}_2\text{F}_4\text{Cl}$  and  $(\text{NH}_4)_3\text{Sn}_5\text{F}_{10}\text{Cl}_3$ ):



or



The observed weight loss of about 12 % seems to indicate that a mixture of ammonium halides, at about 1:1 ratio ( $\text{NH}_4:\text{NH}_4\text{Cl}$ ), is evolved. This is not surprising as both compounds are known to sublime easily. This stage of weight loss is followed by a second and much larger decrease starting at about 350 °C and accelerating very fast above 400 °C, which is believed due to the evaporation of  $\text{SnF}_2$  and  $\text{SnFCl}$ , and as a result no residue is left in the crucible at the end of the experiment.

TABLE 5.3  
Physical constants for the new materials

	<u><math>\text{NH}_4\text{Sn}_2\text{F}_4\text{Cl}/(\text{NH}_4)_3\text{Sn}_5\text{F}_{10}\text{Cl}_3</math></u>	<u><math>\text{K}_3\text{Sn}_5\text{F}_{10}\text{Cl}_3</math></u>
Density, observed (g/cm <sup>3</sup> )	3.63	4.00
Density, calculated (g/cm <sup>3</sup> )	3.43	3.93
Density difference (%)	5.5	1.8
Melting point (°C)	166	235
Colour (crystal)	colourless	colourless
Colour (powder)	white	white
Formula weight (g/mol)	366.825/943.789	1006.789

### 5.7 Physical Constants of New Compounds

The reported values (TABLE 5.3) in this section for the ammonium case were obtained on the mixture of compounds present in the batch (see Section 5.4), whereas in the potassium case, the values stand for pure  $K_3Sn_5F_{10}Cl_3$ . The measured and calculated densities of  $K_3Sn_5F_{10}Cl_3$  are in very good agreement as it is a single phase. On the other hand, the larger density difference obtained for the ammonium sample is attributed to the fact it is a mixture of phases.

---

## 6.0 THE CRYSTAL STRUCTURE OF $(\text{NH}_4)_3\text{Sn}_5\text{F}_{10}\text{Cl}_3$

This chapter presents the structural network and the coordination of individual atoms of the  $(\text{NH}_4)_3\text{Sn}_5\text{F}_{10}\text{Cl}_3$  crystal, which is one of the three new compounds obtained from the  $\text{NH}_4\text{Cl}/\text{SnF}_2$  system.

### 6.1 Method of Choice for Structure Determination

The crystal has a heavy atom (which is tin in this case) in its structure; however, there are a total of three different tin sites with different but very similar environments, in the unit-cell. Two of the three tin species occupy the same symmetry site, while the other does not. This makes it impossible to obtain a set of consistent atomic coordinates, which can be interpreted, from a Patterson map, using the heavy atom method.

The method used to tackle the problem is called the "minimum function" approach, which is more adequate when the structure contains more than one heavy atoms (44). In the minimum function method, the origin of one Patterson map is placed on a peak which corresponds to a vector between two heavy atoms not related by symmetry. It is a trial and error process because the nature of the peaks is unknown until the structure is solved. When the appropriate alignment of maps is found, the places where both maps show a peak reveal an image of the structure.

The crystal structure was finally refined by the block-diagonal least-square technique, with the anisotropic

E. S. Ds. refer to the last digit(s) printed.

	X	Y	Z	BISO
Sn(1)	0	0.99755(12)	0.17409(11)	6.05(20)
Sn(2)	0	0.14698(11)	0.36350(10)	5.77(19)
Sn(3)	0	3/4	0.29497(15)	5.06(20)
Cl(1)	1/2	1/4	0.4102 ( 7)	6.6 ( 6)
Cl(2)	1/2	0.1150 ( 5)	0.1846 ( 5)	7.1 ( 5)
F (1)	0	0.1338 ( 8)	0.4638 ( 8)	5.0 ( 7)
F (2)	1/2	1/4	0.1038 (17)	6.9 (14)
F (3)	0	0.0277 ( 9)	0.0773 ( 8)	5.2 ( 8)
F (4)	0	0.0369 ( 9)	0.3536 ( 8)	5.0 ( 8)
F (5)	1/2	0.1006 ( 8)	0.3721 ( 8)	5.7 ( 8)
F (6)	0	1/4	0.1793 (20)	13.9 (37)
N (1)	0	0	1/2	4.8 (17)
N (2)	0	0.1636 (15)	0.0522 (16)	6.7 (15)

BISO is the arithmetic mean of the principal axes of the thermal ellipsoid.

TABLE 6.1 Final atomic coordinates and equivalent isotropic Debye-Waller factor for  $(\text{NH}_4)_3\text{Sn}_5\text{F}_{10}\text{Cl}_3$ .



E. S. Ds. refer to the last digit(s) printed.

	U11(U)	U22	U33	U12	U13	U23
Sn(1)	11.0( 3)	8.5 ( 3)	3.49(22)	0.00	0.00	0.45(10)
Sn(2)	11.4( 3)	6.40(23)	4.11(22)	0.00	0.00	0.71( 8)
Sn(3)	7.4( 3)	7.3 ( 3)	4.51(25)	0.00	0.00	0.00
Cl(1)	13.3(10)	5.7 ( 6)	5.8 ( 7)	0.00	0.00	0.00
Cl(2)	12.3( 7)	7.2 ( 6)	7.6 ( 6)	0.00	0.00	0.2 ( 5)
F (1)	6.7( 9)	8.6 (11)	3.9 ( 8)	0.00	0.00	-1.4 ( 8)
F (2)	12.3(22)	4.6 (13)	9.3 (20)	0.00	0.00	0.00
F (3)	6.3( 8)	9.2 (13)	4.3 ( 9)	0.00	0.00	-0.6 ( 8)
F (4)	6.7( 9)	7.9 (13)	4.6 ( 9)	0.00	0.00	0.7 ( 7)
F (5)	10.1(11)	4.5 ( 9)	7.3 (11)	0.00	0.00	0.3 ( 8)
F (6)	17.7(43)	28.3 (71)	6.8 (27)	0.00	0.00	0.00
N (1)	8.5(22)	8.4 (25)	1.5 (16)	0.00	0.00	-0.7 (12)
N (2)	7.4(15)	7.6 (18)	10.4 (23)	0.00	0.00	4.6 (16)

TABLE 6.2 Anisotropic ellipsoids of thermal vibration for  $(\text{NH}_4)_3\text{Sn}_5\text{F}_{10}\text{Cl}_3$ .

Bond		Distance (Ångstrom)
Sn1	- F3	2.017(16)
Sn1	- F5	2.254(18)
Sn1	- F4	2.380(08) (x2)
Sn2	- F1	2.005(17)
Sn2	- F4	2.319(19)
Sn2	- F5	2.413(08) (x2)
Sn3	- F2	2.003(33)
Sn3	- F6	2.259(10) (x2)
Sn3	- Cl2	2.863(11) (x2)
F1	- Sn2	2.005(17)
F2	- Sn3	2.003(33)
F3	- Sn1	2.017(16)
F4	- Sn2	2.319(19)
F4	- Sn1	2.380(08) (x2)
F5	- Sn1	2.254(18)
F5	- Sn2	2.413(08) (x2)
F6	- Sn3	2.259(10) (x2)
Cl2	- Sn3	2.863(11) (x2)

TABLE 6.3 Bond distances in  $(\text{NH}_4)_3\text{Sn}_5\text{F}_{10}\text{Cl}_3$ .

Angle				Degree	
F3	-	Sn1	-	F5	84.38 (67)
F3	-	Sn1	-	F4	82.95 (42)
F4	-	Sn1	-	F5	68.20 (43)
F4	-	Sn1	-	F4	135.17 (59)
F1	-	Sn2	-	F4	86.93 (59)
F1	-	Sn2	-	F5	82.78 (42)
F4	-	Sn2	-	F5	66.64 (38)
F5	-	Sn2	-	F5	131.59 (54)
F2	-	Sn3	-	F6	76.95 (97)
Cl2	-	Sn3	-	F2	81.89 (21)
F6	-	Sn3	-	F6	153.91 (1.38)
Cl2	-	Sn3	-	Cl2	163.78 (31)
Cl2	-	Sn3	-	F6	88.18 (14)
Sn1	-	F4	-	Sn2	108.82 (45)
Sn1	-	F4	-	Sn1	135.17 (82)
Sn2	-	F5	-	Sn1	109.91 (41)
Sn2	-	F5	-	Sn2	131.59 (75)
	-	F6	-	Sn3	153.91 (1.95)

TABLE 6.4 Bond angles for  $(\text{NH}_4)_3\text{Sn}_5\text{F}_{10}\text{Cl}_3$ .

factors introduced in the process. A final  $R$  value of 0.0982 ( $R_w = 0.1894$ ) was achieved. The final structural constants are summarized in TABLES 6.1 to 6.4. The  $U_{ij}$  parameters of TABLE 6.2 are the elements of the matrix of root mean square displacement of the atoms.  $U_{ii}$  define the length of the axes of the ellipsoid of thermal vibrations, and  $U_{ij}$  ( $i \neq j$ ) define the orientation of the ellipsoid relative to the crystal axes.

## 6.2 Coordination of the Atoms

The unit-cell of  $(NH_4)_3Sn_5F_{10}Cl_3$  is shown in FIGURE 6.1 (a and b), in two different projections. FIGURE 6.1a corresponds to the  $(\vec{b}, \vec{c})$  plane of the cell, while the  $(\vec{a}, \vec{b})$  plane is shown on FIGURE 6.1b. In addition, a stereoscopic pair of unit-cells is also presented for a three-dimensional viewing useful for a better understanding of the structure (FIGURE 6.2).

There are a total of three different types of tin atoms as mentioned previously, and they are described as below:

- (a) Sn(1)  $SnF_4E$  coordination ( $E =$  lone pair)  
( $sp^3d$  hybridization, pseudotrigonal bipyramid)
- (b) Sn(2)  $SnF_4E$  coordination ( $E =$  lone pair)  
( $sp^3d$  hybridization, pseudotrigonal bipyramid)
- (c) Sn(3)  $SnF_3Cl_2E$  coordination ( $E =$  lone pair)  
( $sp^3d^2$  hybridization, pseudooctahedral)

It should be noted that Sn(1) and Sn(2) have a similar geometry with slightly different bond lengths and angles.

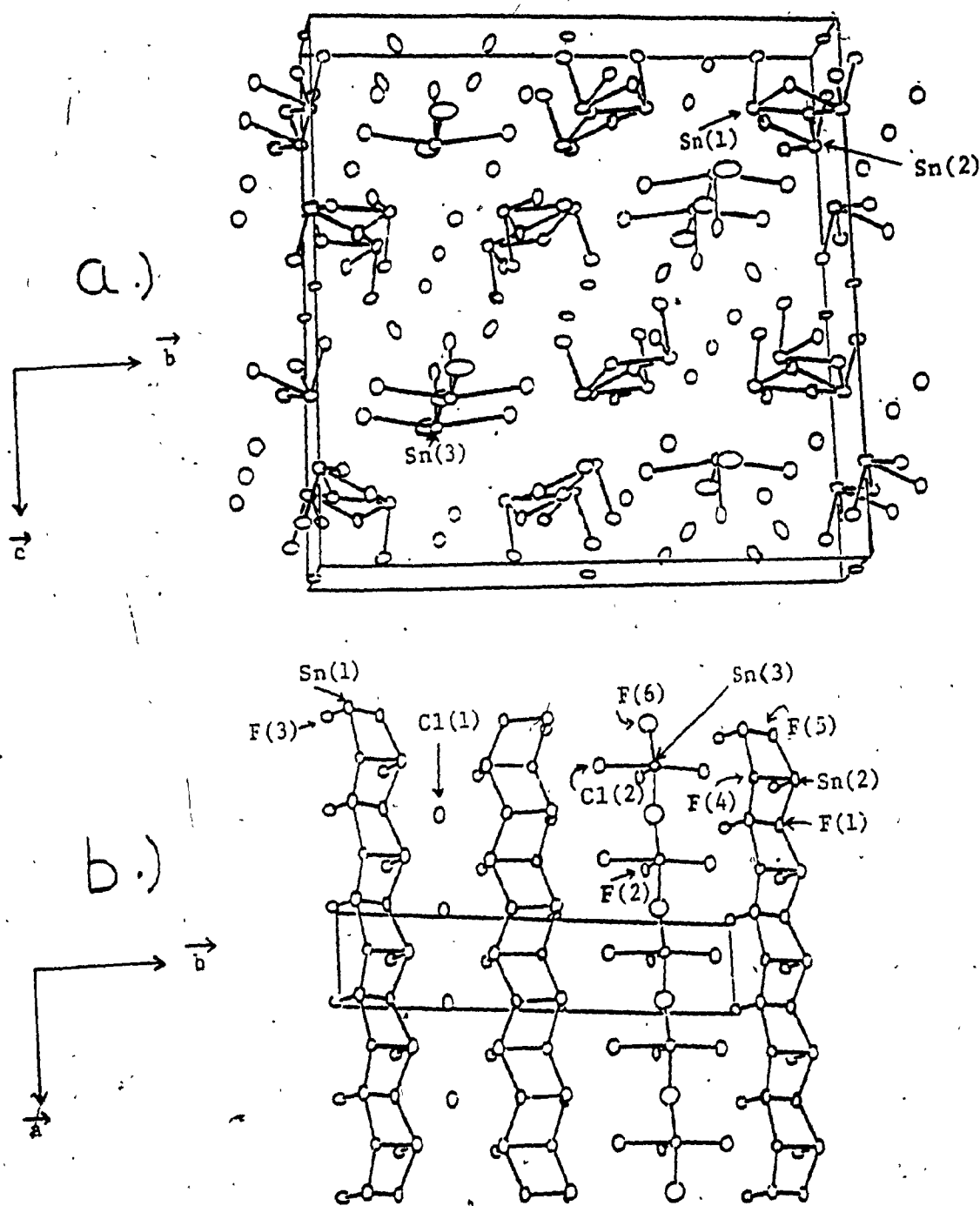


FIGURE 6.1 A unit-cell of  $(\text{NH}_4)_3\text{Sn}_5\text{F}_{10}\text{Cl}_3$ : (a)  $(b, c)$  plane; (b)  $(a, b)$  plane.

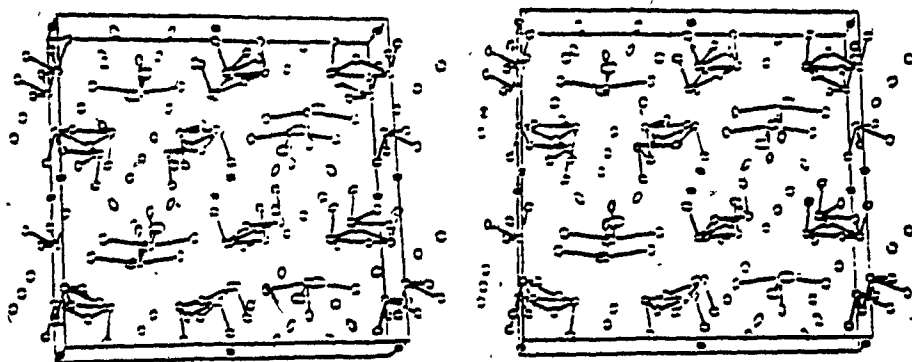
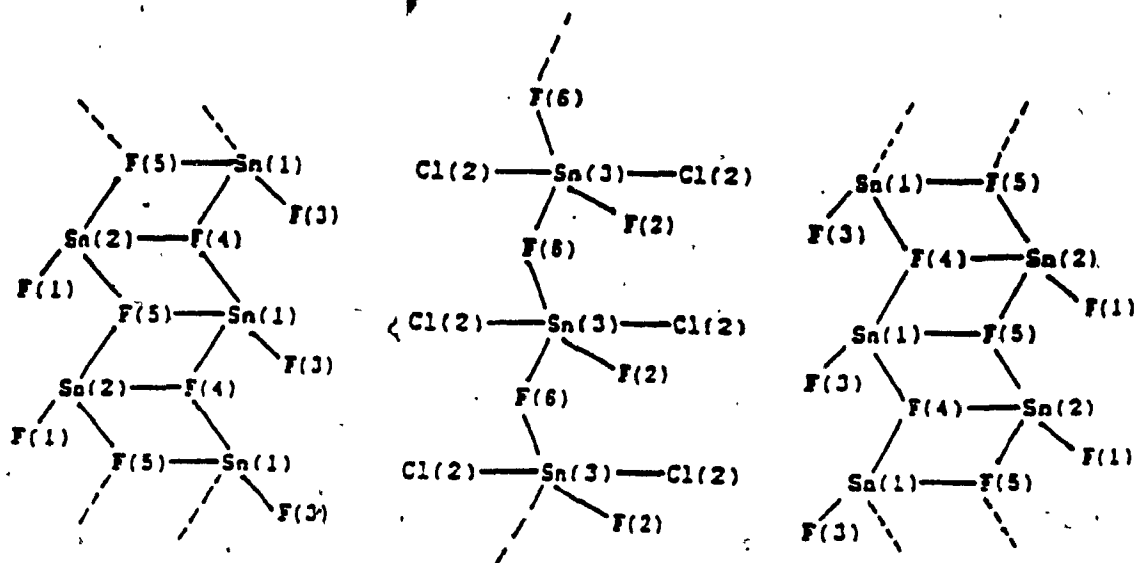
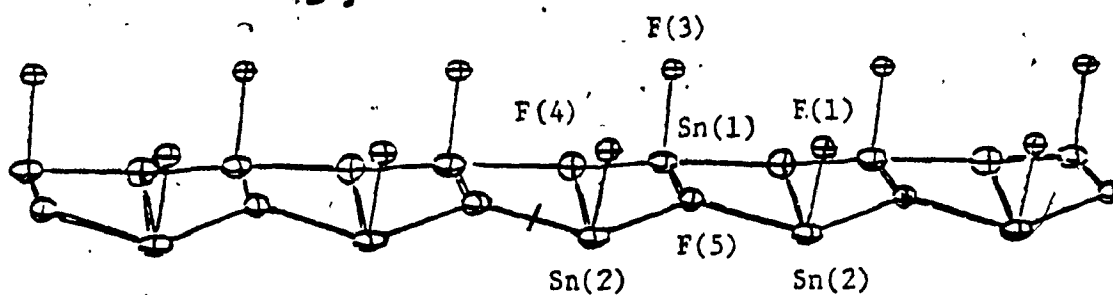


FIGURE 6.2 A stereoscopic pair of  $(\text{NH}_4)_3\text{Sn}_5\text{F}_{10}\text{Cl}_3$  unit-cells.



a.) & b.)



c.)

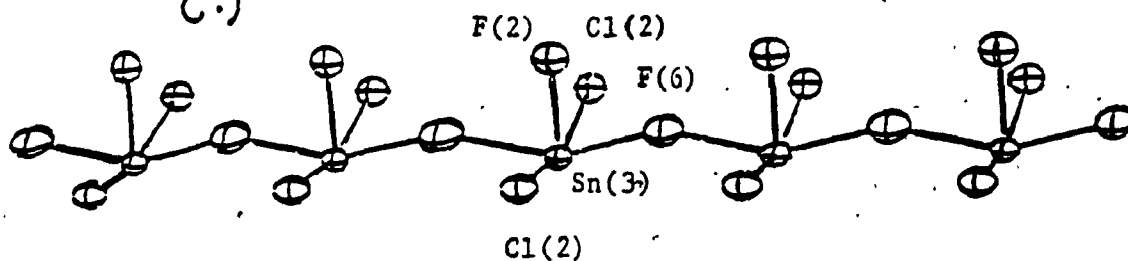


FIGURE 6.3 Coordination of: (a) Sn(1) -  $sp^3d$  hybridization; (b) Sn(2) -  $sp^3d$  hybridization; (c) Sn(3) -  $sp^3d^2$  hybridization.

In the description above, E being the lone pair, the coordination of the three types of tin is shown in FIGURE 6.3 together with a schematic drawing of a repeating unit for a better illustration.

### 6.3 Structural Arrangements of the Atoms

The crystal  $(\text{NH}_4)_3\text{Sn}_5\text{F}_{10}\text{Cl}_3$  crystallizes in an orthorhombic/centrosymmetric space group Bmmb. All the atoms are in special positions. There are four repeating units in a unit-cell (See FIGURE 6.1a). The structure is made of layers of repeating units stacked one above the other. The repeating unit in a layer is  $[(\text{Sn}_2\text{F}_4)^0(\text{SnF}_2\text{Cl}_2)^{2-}(\text{Sn}_2\text{F}_4)^0]^{2-}$  (view from the  $(\vec{b}, \vec{c})$  plane, on FIGURE 6.1a), and each repeating unit is separated from the next by a free chloride ion such that the repeating unit can also be written as  $[(\text{Sn}_2\text{F}_4)^0(\text{SnF}_2\text{Cl}_2)^{2-}(\text{Sn}_2\text{F}_4)^0(\text{Cl})^-]^{3-}$ . The only Sn-Cl bond is observed in the  $(\text{SnF}_2\text{Cl}_2)^{2-}$  sub-units and this is in agreement with the literature (52,53) in terms of Sn-Cl bonding distances. In the repeating unit, there are two tin sites in the  $(\text{Sn}_2\text{F}_4)^0$  sub-units (i.e.  $(\text{Sn}(1)\text{Sn}(2)\text{F}_4)^0$ ) and one in the  $(\text{SnF}_2\text{Cl}_2)^{2-}$  (i.e.  $(\text{Sn}(3)\text{F}_2\text{Cl}_2)^{2-}$ ) for a total of three.

In addition, all the sub-units in a repeating unit (i.e.  $(\text{Sn}_2\text{F}_4)^0$ ,  $(\text{SnF}_2\text{Cl}_2)^{2-}$ , and  $(\text{Cl})^-$ ) are isolated from each other as the way they are written (as seen in FIGURE 6.1a). However, from another projection (FIGURE 6.1b and FIGURE 6.3), it can be visualized that the sub-units



$(\text{Sn}_2\text{F}_4)^0$  and  $(\text{SnF}_2\text{Cl}_2)^{2-}$  form polymer chains through bridging fluorine atoms (F(4), F(5), and F(6), respectively), and not by any chlorine atoms, since they are either isolated (Cl(1)) or terminal (Cl(2)). These polymer chains are aligned along the  $\vec{a}$  axis of the unit-cell.

There are two kinds of  $(\text{NH}_4)^+$  ions and both of them are isolated in a sense that they are not actually bonded to any atoms. One could envisage the existence of hydrogen bonding between these  $(\text{NH}_4)^+$  ions and the terminal fluorine that stick out from the layers (as will be discussed later); however, as no N - F distance shorter than 3.2 Å is present, no such hydrogen bond exists [hydrogen bonded N - F distances in  $\text{NH}_4\text{F}$  is 2.71 Å (54)], and therefore the ammonium ions are rotating. These two types of ammonium ions do not have the same symmetry site, however.

The layers are packed perpendicular to the  $\vec{c}$  axis of the unit-cell and they are described as below:

- at  $z = 0$  and  $3/6$ :  $[(\text{NH}_4)_2]_n^{2n+}$  (Type I)

- at  $z = 0.5/6, 2.5/6, 3.5/6$ , and  $5.5/6$ :

$[(\text{NH}_4)_2]_n^{2n+}$  (Type II)

- at  $z = 1/6, 2/6, 4/6$ , and  $5/6$ :

$[(\text{Sn}_2\text{F}_4)^0(\text{SnF}_2\text{Cl}_2)^{2-}(\text{Sn}_2\text{F}_4)^0(\text{Cl})^{-}]_n^{3n-}$

As mentioned in Section 6.2, there are three different tin species and all of them have a stereoactive lone pair of electrons. Because of these lone pairs, there are constraints on the way each layer is positioned relative to the

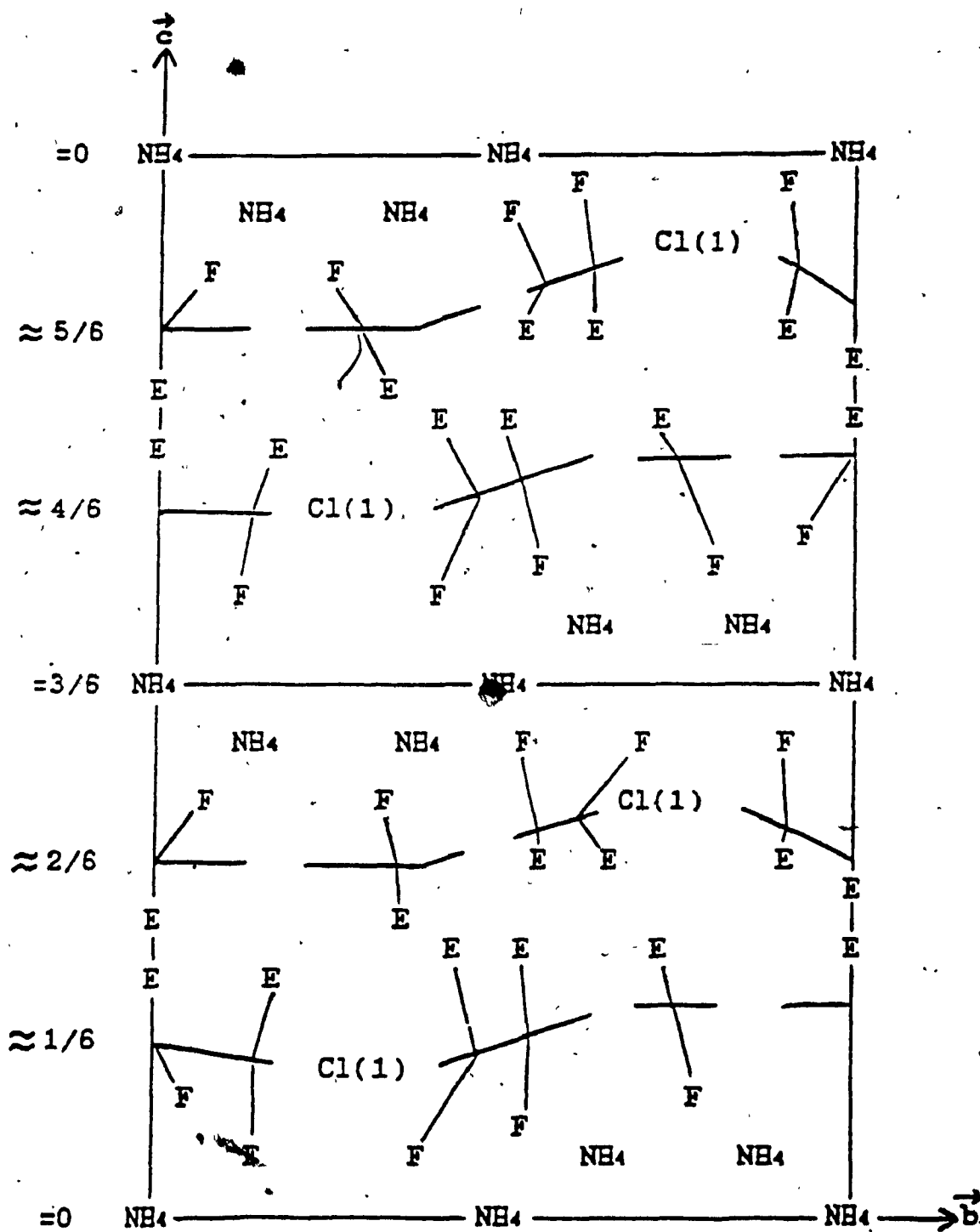


FIGURE 6.4, Schematic plot of a unit-cell of  $(NH_4)_3Sn_5F_{10}Cl_3$  on the  $(b,c)$  plane.

nearest next layer (e.g. layers at  $z = 1/6$  and  $2/6$ ;  $4/6$  and  $5/6$ ).

This extra condition for layer packing is best understood by visual presentation. A schematic illustration, plotted on the  $(\vec{b}, \vec{c})$  plane of the unit-cell, is given (FIGURE 6.4) for that purpose.

In FIGURE 6.4, it can be seen that the repeating units in a molecular layer are separated from each other by a free chloride ion (Cl(1)). The symbol "E" shown in the diagram represents the lone pair of electrons of tin. These tin lone pairs from adjacent molecular layers (i.e. layers at  $z = 1/6$  and  $2/6$ ;  $4/6$  and  $5/6$  only) are pointing towards the inner-layer spacing and keeping the layers apart. The strong repulsions between the tin(II) lone pairs of adjacent layers are responsible for the cleavage behaviour, resulting in crystals shaped as thin long platelets.

All the terminal fluorine (F(1), F(2), and F(3), symbolized as "F" in the diagram), are sticking out of the layers in directions opposite to the lone pairs, such that hydrogen bonding to the free  $(\text{NH}_4)^+$  ions is possible, but seems not to be present in this structure at room temperature. Therefore, there are only Van der Waals interactions between the layers which explains the low melting point of the compound (Sections 5.6 and 5.7).

## 7.0 DISCUSSION

### 7.1 Results Interpretation

#### 7.1.1 Crystallographic study

Various experimental results obtained throughout this research are definitely evidence for the co-existence of several ammonium-tin-halo complexes from the system  $\text{NH}_4\text{Cl}/\text{SnF}_2$  (at least three of them have been identified thus far). Two of the three different complexes have yet to be looked at in depth; therefore, the analogy here is stressed on  $(\text{NH}_4)_3\text{Sn}_5\text{F}_{10}\text{Cl}_3$ , along with the new unique compound obtained from the  $\text{KCl}/\text{SnF}_2$  system,  $\text{K}_3\text{Sn}_5\text{F}_{10}\text{Cl}_3$ .

The physical appearance of the two compounds are shown in FIGURE 5.1. They exist as long needle-shaped crystals. The crystal growth is in agreement with the law of Bravais on crystal morphology (55) that is a short axis of the unit-cell corresponds a long axis of crystal growth and vice-versa, such that the crystal shape resembles the shape of the reciprocal cell. For the ammonium-containing crystals, the plane perpendicular to  $\vec{c}$  axis have an area of about  $0.08 \text{ mm}^2$ , while the potassium-containing needles are leaner (about  $0.005 \text{ mm}^2 = \text{area of the same plane}$ ). This crystal shape originates in the bonding anisotropy, as explained in the Paragraph 6.3.

Oscillation photographs gave the periodicity along the main axis of the needle ( $\vec{a}$  axis, about  $4.4 \text{ \AA}$  for both compounds), while Weissenberg and precession photographs showed the two other axes to be very long (approximately

20.5 Å and 19.5 Å for  $\vec{b}$  and  $\vec{c}$ , respectively) and the angles  $\alpha = \beta = \gamma = 90^\circ$ , suggesting the cell is orthorhombic. Laue photographs showed the Laue group is mmm for both compounds, hence confirming the orthorhombic symmetry.

The diffraction pattern observed from Weissenberg and precession photographs for both compounds are identical (except for small differences in terms of periodicities). The absence conditions determined from the photographs showed that the conditions for Bragg peaks to be observed are listed as below:

(h00):  $h = 2n$ ; (hk0):  $h = 2n, k = 2n, h + k = 2n$ ;

(0k0):  $k = 2n$ ; (0kl):  $k = 2n, l = 2n, k + l = 2n$ ;

(00l):  $l = 2n$ ; (h0l):  $h = 2n, l = 2n, h + l = 2n$ ;

(hkl):  $h + l = 2n$

The condition on the (hkl) planes indicates the Bravais lattice is B-face centered. From the above conditions, three possible space groups were determined for both compounds and they were  $Bm2_1b$  (Number 36),  $B2mb$  (Number 40), and  $Bmmb$  (Number 63).

However, after the crystal structure analytical work for  $(NH_4)_3Sn_5F_{10}Cl_3$ , it has been confirmed that the compound indeed crystallizes in the space group  $Bmmb$ . Since this compound has the same stoichiometry as the potassium salt,  $K_3Sn_5F_{10}Cl_3$ , their diffraction patterns are identical, and the ionic radii of  $K^+$  and  $NH_4^+$  are similar, it is very likely that  $K_3Sn_5F_{10}Cl_3$  also crystallizes in the space group

Bmmb. That is to say, these two compounds could indeed be iso-structural at room temperature.

#### 7.1.2 Mössbauer spectroscopic analysis

The  $^{119}\text{Sn}$  Mössbauer isomer shifts and quadrupole splittings for the new compounds from this research are presented, along with that of other related compounds, in TABLE 5.2. Although the products obtained from the  $\text{NH}_4\text{Cl}/\text{SnF}_2$  system appear to be a mixture of several species, the presentation here refers to the overall for the batch.

Close examination of the spectral data reveals that they are characteristic of divalent tin with a stereoactive lone pair of electrons. Such a lone pair is localized on a non-bonding orbital; therefore, it occupies a volume similar to that of a fluoride ion in the structure (33) and it cannot populate conduction bands to give rise to electronic conduction unless tin is surrounded by Br or I in a highly symmetrical environment (32). The latter case gives rise to very high isomer shifts ( $\delta \approx 4 \text{ mm.s}^{-1}$ ) due to the high s, contribution to the lone pair, and very small quadrupole splittings ( $\Delta \approx 0 \text{ mm.s}^{-1}$ ) due to the absence of p contribution to the lone pair and high site symmetry at tin, such that the electric field gradient (e.f.g.) at tin is nearly zero (31). A large  $p_z$  contribution to the lone pair of tin gives a large e.f.g. at tin, therefore a large valence contribution to the splitting results. The lattice contribution being small, it is usually negligible and is often masked by the valence contribution which is much

larger and often of opposite sign. This is probably why the two tin sites are indistinguishable by Mössbauer spectroscopy in  $\alpha$ - $\text{SnF}_2$  (56) and in  $\text{KSn}_2\text{F}_5$  (21,57). It has been confirmed that there are a total of three different tin sites in the compound  $(\text{NH}_4)_3\text{Sn}_5\text{F}_{10}\text{Cl}_3$  (Chapter Six), and if in fact  $\text{K}_3\text{Sn}_5\text{F}_{10}\text{Cl}_3$  and  $(\text{NH}_4)_3\text{Sn}_5\text{F}_{10}\text{Cl}_3$  are isostructural (See Section 7.1.1), then there should also be three different tin sites in the potassium case. In these two compounds, even though the three tin sites are non-equivalent, structure analysis shows that they all are dominated by the stereoactivity of the lone pair (Chapter Six). Therefore, their respective isomer shifts are so close to each other (or perhaps even overlap with each other), resulting in "line-broadening" in the Mossbauer spectrum. The fact that the doublet observed for  $(\text{NH}_4)_3\text{Sn}_5\text{F}_{10}\text{Cl}_3$  (FIGURE 5.2 d and e) is not symmetric is not surprising, since the patch was a mixture of different species and just  $(\text{NH}_4)_3\text{Sn}_5\text{F}_{10}\text{Cl}_3$  contains three tin sites, there are probably several non-equivalent tin sites overall and as a result the range of isomer shifts and quadrupole splittings is wider.

Therefore, the fact that only one divalent tin site is seen in Mössbauer spectroscopy cannot be used to predict the number of tin sites in these compounds. However, the Mössbauer parameters are safe probes for the absence of electronic density being promoted from the lone pair to the conduction band, the gap energy being too high for fluorides

and chlorides, especially when no large cation such as  $\text{Cs}^+$  is present. As a result, if electric conductivity is present in these new compounds, it will likely be ionic in nature, due to the long range motion of fluoride ions in the solid (13,58).

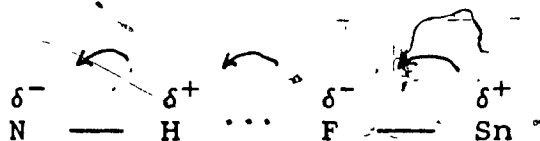
Donaldson and Senior (59) have shown that a quasi-linear relationship exists between the isomer shift and the quadrupole splitting of iso-structural divalent tin compounds, i.e. for compounds having a similar tin (II) coordination. This is easily explained by the fact that the value of the isomer shift is proportional to the amount of s electron density at tin and the quadrupole splitting to the amount of  $p_z$  electron density in the lone pair (the lattice contribution to the quadrupole splitting being often negligible and should be similar for iso-structural compounds).

Generally speaking, for Sn-X bonds, the higher the electronegativity of X, the more the s electron density pulled away from tin, and therefore the lower the isomer shift.

The larger isomer shift and smaller quadrupole splitting observed for the batch of ammonium complexes, as compared to  $\text{K}_3\text{Sn}_5\text{F}_{10}\text{Cl}_3$ , could have been explained by p electron density withdrawing from tin through hydrogen bonding to fluorine as shown below, which cannot occur in the potassium case. However, as the crystal structure analysis shows there is no hydrogen bonding at room



temperature, another phenomenon, probably structural, is responsible for the ammonium complex values.



## 7.2 Comparison between this research and the earlier similar systems

Research areas involving alkali metal halides and stannous fluoride have been undergoing for almost three decades, and many new materials have been identified. These new materials, such as  $\text{NaSn}_2\text{F}_5$  (20),  $\text{KSn}_2\text{F}_5$  (21), and  $\text{NH}_4\text{Sn}_2\text{F}_3$  (22), do not crystallize in any orthorhombic space groups.

However, the new compounds from this research (except one of the three complexes from the  $\text{NH}_4\text{Cl}/\text{SnF}_2$  system), all have a Laue group  $\text{mmm}$ , confirming they belong to the orthorhombic system. The difference between fluorides and chlorofluorides is definitely related to the introduction of a different halide (which is chloride in this case) with a larger ionic radius and a smaller electronegativity.

The Mössbauer spectral data confirmed that the new materials from this research do not have any semi-conducting properties, which are the features for materials like  $\text{CsSnBr}_3$  and  $\text{CsSnCl}_3$  (14). Indeed, these new materials, at least from the Mössbauer spectral point of view, should behave like the  $\text{MSn}_2\text{F}_5$  family.

The similarities and differences between them are examined in the next two sections.

### 7.3 Effect of different halides on physical properties

As once stated, materials obtained from the  $\text{MX/SnF}_2$  systems ( $\text{X} = \text{F}, \text{Br}, \text{and I}$ ) have different physical behaviours (e.g. electrical and physical appearance) depending on the nature of the halide involved, as the more electronegative fluorine gives rise to white ionic conducting materials and the less electronegative bromine and iodine result in semiconducting and strongly coloured compounds.

Such a marked difference can be depicted by their respective Mössbauer spectral data (TABLE 5.2).

The values for  $\text{M}_3\text{Sn}_5\text{F}_{10}\text{Cl}_3$  ( $\text{M} = \text{K}$  and  $\text{NH}_4$ ) are comparable to those for the ionic conductors  $\alpha\text{-SnF}_2$  (56) and  $\text{MSn}_2\text{F}_5$  ( $\text{M} = \text{K}$  and  $\text{NH}_4$ ) (57) (spectrum b of FIGURE 4.3). In addition, the white colour indicates no visible light absorption, showing absence of population in the conduction band. It can therefore be concluded, just based on the Mössbauer data, that the  $\text{M}_3\text{Sn}_5\text{F}_{10}\text{Cl}_3$  compounds are highly unlikely to have significant semiconducting properties at room temperature. For the  $\text{SnF}_2/\text{MI}$  systems ( $\text{M} = \text{K}$  and  $\text{NH}_4$ ), when the compounds are rich in fluorine ( $\text{F/I} = 6$  and  $4$ ), the isomer shifts and quadrupole splittings are similar to that of the fluorides, indicating no electron transfer to the conduction band of tin. In such a case, the yellow colour is accounted for by the self population of empty orbitals of

iodine by iodine electrons as in iodine element. Therefore, these compounds are most likely to be insulators or ionic conductors, as are  $\alpha$ - $\text{SnF}_2$  and probably the  $\text{M}_3\text{Sn}_5\text{F}_{10}\text{Cl}_3$  compounds. On the other hand, for the fluoroiodides richer in iodine ( $\text{F/I} = 2$ ), two tin(II) sites are present with one similar to that observed when  $\text{F/I} = 6$  and 4, but the other with  $\delta = 4.0$  and  $\Delta = 0$ , indicating an octahedral coordination of tin, where the tin lone pair is on a pure  $5s^2$  orbital. These compounds are more highly coloured (orange) and can be suspected to be semiconductors. For large alkali metals, mostly cesium, and for less electronegative halides, i.e. Br and I, the amount of p contribution to the lone pair decreases and often reaches zero to give a pure  $5s^2 5p^0$  spherical lone pair. In such compounds, the band gap is low, resulting in a significant population of the conduction band, giving rise to semiconducting behaviour and strongly coloured materials.

#### 7.4 Ionic radii and structural analogies

The unit-cells for  $\text{KSn}_2\text{F}_5$  and  $\text{NH}_4\text{Sn}_2\text{F}_5$  were first reported by Donaldson and O'Donoghue (16) to be orthorhombic and pseudohexagonal, respectively. In 1967, Goost and Bergerhoff reported  $\text{KSn}_2\text{F}_5$  crystallizes in the  $P3$  hexagonal space group. More recent works give a monoclinic cell (pseudoorthorhombic:  $\beta = 90.09^\circ$ ) for  $\text{KSn}_2\text{F}_5$  (18). Finally, its structure was solved in the trigonal  $P3$  space group (21). The latest cell for  $\text{NH}_4\text{Sn}_2\text{F}_5$ , however, was reported

to be monoclinic (30) with  $\beta = 103.52^\circ$ . Close examination of the trigonal cell of  $\text{KSn}_2\text{F}_5$  shows an analogy with the orthorhombic cells of  $\text{K}_3\text{Sn}_5\text{F}_{10}\text{Cl}_3$  and  $(\text{NH}_4)_3\text{Sn}_5\text{F}_{10}\text{Cl}_3$  (TABLE 7.1, FIGURE 7.1). When one  $\text{SnF}_2$  molecule is removed from  $\text{K}_3\text{Sn}_6\text{F}_{15}$  (i.e.  $3\text{KSn}_2\text{F}_5$ ), and three fluorine atoms are replaced by three chlorine atoms,  $\text{K}_3\text{Sn}_5\text{F}_{10}\text{Cl}_3$  is obtained. As we have shown above (Section 7.1.1) that  $\text{K}_3\text{Sn}_5\text{F}_{10}\text{Cl}_3$  and  $(\text{NH}_4)_3\text{Sn}_5\text{F}_{10}\text{Cl}_3$  are most likely isostructural, one can compare the structures of  $\text{K}_3\text{Sn}_6\text{F}_{15}$  (i.e.  $3\text{KSn}_2\text{F}_5$ ) and  $\text{K}_3\text{Sn}_5\text{F}_{10}\text{Cl}_3$ .

TABLE 7.1  
Comparison of the unit-cells between  $\text{M}_3\text{Sn}_5\text{F}_{10}\text{Cl}_3$  and  $\text{KSn}_2\text{F}_5$   
( =  $\text{K}_3\text{Sn}_6\text{F}_{15}$ )

<u><math>\text{K}_3\text{Sn}_5\text{F}_{10}\text{Cl}_3</math></u>	<u><math>\text{K}_3\text{Sn}_6\text{F}_{15}^{**}</math></u> ( $\text{KSn}_2\text{F}_5$ )	<u><math>(\text{NH}_4)_3\text{Sn}_5\text{F}_{10}\text{Cl}_3</math></u>
$a = 4.358 \text{ \AA}$	$(2/3)a_h \cos 30^\circ = 4.209 \text{ \AA}$	$a = 4.401 \text{ \AA}$
$b = 20.346 \text{ \AA}$	$3a_h = 21.873 \text{ \AA}$	$b = 20.999 \text{ \AA}$
$c = 19.204 \text{ \AA}$	$2c_h = 19.722 \text{ \AA}$	$c = 19.794 \text{ \AA}$
$V = 1702.778 \text{ \AA}^3$	$V = 1815.676 \text{ \AA}^3$	$V = 1829.294 \text{ \AA}^3$
$Z = 4$	$Z = 4$	$Z = 4$
$V_Z = 425.694 \text{ \AA}^3$	$V_Z = 453.92 \text{ \AA}^3$	$V_Z = 457.324 \text{ \AA}^3$
$\alpha = \beta = \gamma = 90^\circ$	$\alpha = \beta = 90^\circ; \gamma = 120^\circ$	$\alpha = \beta = \gamma = 90^\circ$
orthorhombic	trigonal	orthorhombic
Reference: TW*	Reference: 21	Reference: TW*

\* TW = This work

\*\*  $a_h, c_h$  = hexagonal axes. The orthorhombic supercell is given for comparison.

TABLE 7.1 shows that the cell of  $K_3Sn_6F_{15}$  is 3.4 % shorter in the  $\vec{a}$  direction; however, it is 7.5 % longer along  $\vec{b}$  and 2.7 % longer along  $\vec{c}$ , such that its volume is 6.6 % larger. These changes are the sum of the two differences in composition in difference between the two compounds. As  $K_3Sn_5F_{10}Cl_3 = K_3Sn_6F_{15} - SnF_2 - 1.5SnF_2 + 1.5SnCl_2$ ,  $K_3Sn_5F_{10}Cl_3$  can be considered as a variation of  $K_3Sn_6F_{15}$  in which has been removed and 1.5 $SnF_2$  have been replaced by 1.5 $SnCl_2$ . Removing one  $SnF_2$  should result in a volume decrease of about 53.3 Å<sup>3</sup> (33), while replacing 3 $SnF_2$  by 3 $SnCl_2$  gives a volume increase of 78.48 Å<sup>3</sup>, based on the volume occupied by one  $SnF_2$  in  $\alpha$ - $SnF_2$  (53.3 Å<sup>3</sup>) and one  $SnCl_2$  in orthorhombic  $SnCl_2$  (79.46 Å<sup>3</sup>) (53). It results that the expected volume of the unit-cell of  $K_3Sn_5F_{10}Cl_3$  is  $1815.676 - 53.3 + 78.48 = 1840.18$  Å<sup>3</sup>. However, the observed cell volume of  $K_3Sn_5F_{10}Cl_3$  is 1702.778 Å<sup>3</sup>, i.e. 8.1 % lower than expected. Although this is a crude calculation and it depends on the efficiency of packing of  $\alpha$ - $SnF_2$  and  $SnCl_2$ , it clearly shows that packing is more efficient in  $K_3Sn_5F_{10}Cl_3$  than in  $K_3Sn_6F_{15}$ . As shown in TABLE 7.1 and on FIGURE 7.1, stacking of the layers perpendicular to  $\vec{c}$  results in less dead space between the layers, despite strong repulsion between the tin layers in both structures. There is also a most efficient packing within the layers: in the  $\vec{b}$  direction, it is about three times more efficient than perpendicular to the layers, whereas the efficiency is lower along  $\vec{a}$ , where the periodicity is 3.4 % longer in  $K_3Sn_5F_{10}Cl_3$ ,

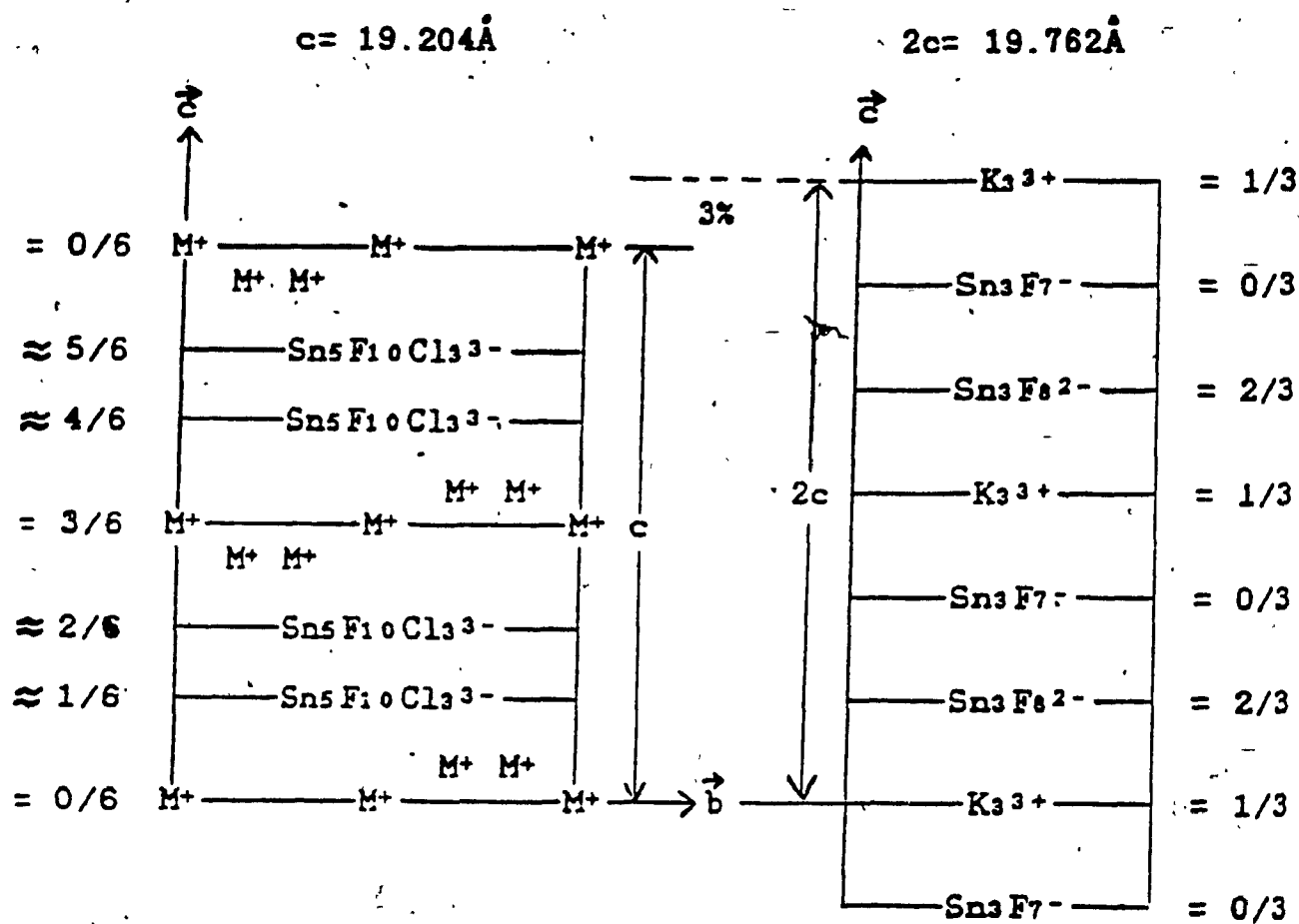


FIGURE 7.1 Relationships between the cell of trigonal  $\text{KSn}_2\text{F}_5$  and the orthorhombic cells of  $\text{M}_3\text{Sn}_5\text{F}_{10}\text{Cl}_3$  ( $\text{M} = \text{K}$  and  $\text{NH}_4$ ).

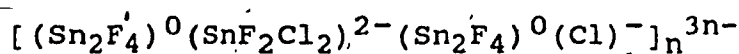
when a 2 % lengthening would be expected for an isotropic volume increase of 8.1 %. However, no isotropic effect should be expected in these highly anisotropic structures. The differences observed arise from the different composition and structure of the layers. The layer sequence is similar in both compounds (FIGURE 7.1). For  $\text{KSn}_2\text{F}_5$ , one finds:

- at  $z = 0$ :  $(\text{Sn}_3\text{F}_7)_n^{n-}$
- at  $z = 1/3$ :  $(\text{K}_3)_n^{3n+}$
- at  $z = 2/3$ :  $(\text{Sn}_3\text{F}_8)_n^{2n-}$

The main differences between the two structures are the presence of chlorine in the tin-fluorine layers and the non-planarity of the potassium layers.

In the case of  $\text{K}_3\text{Sn}_5\text{F}_{10}\text{Cl}_3$ , the stacking of layers can be described as follows (See Chapter Six):

- at  $z = 0$  and  $3/6$ :  $(\text{K}_2)_n^{2n+}$
- at  $z = 0.5/6, 2.5/6, 3.5/6$ , and  $5.5/6$ :  $(\text{K}_2)_n^{2n+}$
- at  $z = 1/6, 2/6, 4/6$ , and  $5/6$ :



$\text{K}_3\text{Sn}_5\text{F}_{10}\text{Cl}_3$  is a two-dimensional superstructure of  $\text{KSn}_2\text{F}_5$ . The superstructure along  $\vec{c}$  is clearly visible on FIGURE 7.1.

### 7.5 Further work

The present study shows how the electrical properties of divalent tin compounds are directly related to tin(II) electronic structure. The effect of the nature of the

halides and other cation on physical properties and crystal structures have also been described.

The present project was undertaken as an attempt to compare the chloride containing compounds to the hitherto known fluorides, bromides, and iodides. Perhaps, it is useful at this stage, to propose an extension to the present study.

The crystal structure of  $K_3Sn_5F_{10}Cl_3$  has yet to be determined, although there are good reasons to believe it is isostructural to  $(NH_4)_3Sn_5F_{10}Cl_3$ . It would definitely be an asset to know this structure in order to compare the relations between the two compounds and see the effect of hydrogen bonding in the ammonium case upon lowering the temperature.

In addition, ammonium chloride/stannous fluoride solutions seem to give several different complex species. It would be interesting to see how these relate to each other and whether they are different species, polymorphs or polytypes.

It would also be interesting to solve the structure of  $(NH_4)_3Sn_5F_{10}Cl_3$  and the other ammonium-containing compounds at low temperature, in order to freeze the rotation of the ammonium ions and see how hydrogen bonding to the terminal fluorine atoms is formed. Therefore, at low temperature, ammonium ions could establish links between the tin-fluorine planes, via hydrogen bonding bridges. However, strong repulsions in the planes of lone pairs would remain, and



therefore, strong texture effects would still be expected to take place.

Another type of investigation that should be concentrated on for our new materials is the study of their electrical properties. Conductivity measurements and ionic transport measurements should be performed for these materials in order to check whether they are indeed ionic conductors and to study their conducting properties in detail.

Solid state synthesis for the three systems studied in this project have also been done as a preliminary investigation to see whether new products can be obtained via such route and the results were confirmed to be positive. Since our new materials have been prepared by solid state synthesis using exact stoichiometric amount of reagents, the stoichiometry of the products is known, provided one phase only is obtained, therefore, comparison of the X-ray powder diffraction patterns of the samples obtained by solid state reactions and from aqueous solutions can be used to find the stoichiometry of the crystals obtained from aqueous solutions. In addition, solid state reactions can give products inaccessible from aqueous solutions because of competition between the crystal growth of different species of similar solubility. Finally, solid state reactions can also give high temperature phase, obtained in the metastable state at room temperature upon quenching from high temperature.

Mössbauer spectroscopy for these new products at high and low temperatures are worth doing, since valuable information can be obtained, such as changes in coordination of tin sites if phase transitions take place. In addition, changes of isomer shifts, and recoil-free fraction can be related to the lattice dynamics.

Certainly there are many directions that can be taken for tin research and what we have mentioned here are just a few of the very many.

## REFERENCES

1. B. Kolk, in "Dynamic Properties of Solids, Volume 5: Mössbauer Effect, Structural Phase Transitions", G.K. Horton and A.A. Maradudin, Eds., North Holland, Amsterdam, 1984, 500 pages, pp. 99-101.
2. P. Boolchand and M. Stevens, Phys. Rev. B29, 1 (1984).
3. R.C.T. Slade, M.G. Cross, and W.A. England, Solid State Ionics, 6, 225 (1982).
4. R. Lalauze, J.C. Le Thièssé, C. Pijolat, and M. Soustelle, Solid State Ionics, 12, 453 (1984).
5. D. Bélanger, M. Bartkowski, J.-P. Dodelet, B.A. Lombos, I. Dickson, and L. Dao, J. Can. Ceram. Soc., 52, 28 (1983).
6. J.P. Joly, L. Gonzalez-Cruz, and Y. Arnaud, Bull. Soc. Chim. Fr., Number 1, 11 (1986).
7. K.M. Rabe and J.D. Joannopoulos, Phys. Rev., B32, 2302 (1985).
8. E. Asmus, A. Bull, and E. Wollsdorf, Z. Anal. Chem., 193, 81 (1963).
9. K.V. Astakhov and I.E. Bukolov, Z. Neorgan. Khim., 7, 2082 (1962).
10. V. Auger and T. Karantassis, Compt. Rend., 180, 1845 (1925).
11. J.D. Donaldson, in "Progress in Inorganic Chemistry, Volume 8: The Chemistry of Bivalent Tin", F. Albert Cotton, Ed., Interscience Publishers, New York, 1967, 488 pages, pp. 287-356.

12. E.W. Abel, in "Comprehensive Inorganic Chemistry, Volume 2", J.C. Bailar, H.J. Emeléus, Sir Ronald Nyholm, and A.F. Trotman-Dickenson, Eds., Pergamon Press, Oxford, 1973, p. 51.
13. G. Dénès, T. Birchall, M. Sayer, and M.F. Bell, Solid State Ionics, 13, 213 (1984).
14. J. Barrett, S.R.A. Bird, J.D. Donaldson, and J. Silver, J. Chem. Soc., (A), 3105 (1971).
15. H. Kriegsmann and G. Kessler, Z. Anorg. Chem., 318, 266 (1962).
16. J.D. Donaldson and J.D. O'Donoghue, J. Chem. Soc., Chem. Comm., 271 (1974).
17. L. Goost and G. Bergerhoff, Naturwissenschaften, 54, 248 (1967).
18. L. Lavassani Abbas, G. Jourdan, C. Avinens, and L. Cot, C.R. Acad. Sc. Paris, 279C, 307 (1974).
19. A. Lari Lavassani, L. Cot, C. Geneys, and C. Avinens, C.R. Acad. Sc. Paris, 280C, 1211 (1975).
20. R.R. McDonald, A.C. Larson, and D.T. Cromer, Acta Cryst., 17, 1104 (1964).
21. S. Vilminot, R. Bachmann, and H. Schulz, Solid State Ionics, 9&10, 559 (1983).
22. G. Bergerhoff and L. Goost, Acta Cryst., B29, 632 (1973).
23. E. Acker, K. Recker, and S. Haussühl, J. Cryst. Growth, 35, 165 (1976).

24. G. Bergerhoff and H. Namgung, *Acta Cryst.*, B34, 699 (1978).
25. G. Berherhoff, L. Goost, and E. Schultze-Rhonhof, *Acta Cryst.*, B24, 803 (1968).
26. G. Berherhoff and L. Goost, *Acta Cryst.*, B26, 19 (1970).
27. S. Vilminot, G. Pérez, W. Granier, and L. Cot, *Rev. Chimie Miner.*, 17, 397 (1980).
28. W.D. Basler, I.V. Murin, and S.V. Chernov, *Z. Naturforsch.*, 86a, 519 (1981).
29. W. Granier, P. Bernier, M. Dohri, J. Alizan, and H. Robert, *J. Physique*, 42, L301 (1981).
30. J.P. Battut, J. Dupuis, H. Robert, and W. Granier, *Solid State Ionics*, 8, 77 (1981).
31. J.D. Donaldson and J. Silver, *J. Chem. Soc.*, (A), 666 (1973).
32. J.D. Donaldson and J. Silver, *J. Solid State Chem.*, 18, 117 (1976).
33. G. Dénès, J. Pannetier, J. Lucas, and J.Y. Le Marouille, *J. Solid State Chem.*, 30, 335 (1979).
34. T. Birchall and G. Dénès, *Can. J. Chem.*, 62, 591 (1984).
35. E.S. Gladney and W.E. Goods, *Anal. Chim. Acta*, 91, 411 (1977).
36. W.M. Latimer and J.H. Hildebrand, "Reference Book of Inorganic Chemistry", 3rd Edition, Macmillan Co., New York, 1964, p. 198.

37. H.A. Laitinen, "Chemical Analysis: An Advanced Text and Reference", McGraw Hill, New York, 1960, pp. 198-199.
38. E.J. Gabe, "LSTSQ - NRC Program".
39. E.J. Gabe, "FOURR - NRC Program".
40. E.J. Gabe, "DISPOW - NRC Program".
41. C.K. Johnson, "ORTEP - Oak Ridge Thermal Ellipsoid Program", Oak Ridge National Laboratory, Oak Ridge, Tennessee, 1966.
42. K. Ruebenbauer and T. Birchall, Hyperfine Int., 7, 125 (1979).
43. J. Monnier, G. Dénès, and R.B. Anderson, Can. J. Chem. Eng., 62, 419 (1984).
44. J.P. Glusker and K.N. Trueblood, "Crystal Structure Analysis, A Primer", 2nd Edition, Oxford University Press, New York, 1985, 269 pages.
45. G.H.W. Milburn, "X-ray Crystallography, An Introduction to the Theory and Practice of Single-Crystal Structure Analysis", Butterworth & Co. Publishers Ltd., London, 1973, 217 pages.
46. J.C. Speakman, "Molecular Structure: Its Study by Crystal Diffraction", The Chemical Society Monographs for Teachers, Number 30, Bartholomew Press, Dorking, 1977, 51 pages.
47. A.M. Legendre, "Nouvelles Méthodes pour la Détermination des Orbites des Comètes", Courcier, Paris, 1806, p. 72.

48. T.C. Gibb, "Principles of Mössbauer Spectroscopy", Chapman and Hall Ltd., London, 1980, 254 pages.
49. N.N. Greenwood and T.C. Gibb, "Mössbauer Spectroscopy", Chapman and Hall Ltd., London, 1971, 659 pages.
50. H.J. Lipkin, Ann. Phys., 9, 332 (1960).
51. V.G. Bergerhoff and L. Goost, Acta Cryst., B30, 1362 (1974).
52. J.D. Donaldson, D.R. Laughlin, and D.C. Puxley, J. Chem. Soc., (A), Dalton Tr., 865 (1977).
53. J.M. Van Den Berg, Acta Cryst., 14, 1002 (1961).
54. H.D. Megaw, "Crystal Structures. A Working Approach", W.B. Saunders Co., London, 1973, pp. 502-507.
55. J.D.H. Donnay and D. Harker, Am. Mineralogist, 22, 446 (1937).
56. T. Birchall, G. Dénès, K. Reubenbauer, and J. Pannetier, J. Chem. Soc., Dalton Tr., 1831 (1981).
57. J.D. Donaldson and B.J. Senior, J. Chem. Soc., (A), 1798 (1966).
58. D. Ansel, J. Debuigne, G. Dénès, J. Pannetier, and J. Lucas, Ber. Bunsenges. Phys. Chem., 82, 376 (1978).
59. J.D. Donaldson and B.J. Senior, J. Inorg. Nucl. Chem., 31, 881 (1969).